ABSTRACT

Title of Thesis: IMPROVEMENTS IN MICROBOILING DEVICE DESIGN

Michael J. Carrier, Master of Science, 2011

Directed By: Professor Gary W. Rubloff
Department of Materials Science and Engineering

Small ribbon heaters (10 μm – 20 μm wide) have been used for many years to study the formation of microbubbles in liquids when short voltage pulses are applied. This thesis describes improvements in the device design with an emphasis on smaller and more sensitive heaters. I used a novel method of creating 250 nanometer wide heaters to keep both the fabrication time and costs as low as possible by using a focused ion beam to create the heaters from a set of larger devices. Ribbon heaters are usually fabricated on a thin SiO_2 layer on a silicon wafer which acts as a large heat sink whose effect becomes more pronounced the smaller the heater width. Suspending the heaters on a thin membrane dramatically increased their sensitivity in microboiling experiments. The suspended devices required the development of a very low stress platinum deposition process.

IMPROVEMENTS IN MICROBOILING DEVICE DESIGN

By

Michael James Carrier

Thesis submitted to the Faculty of the Graduate School of the
University of Maryland, College Park, in partial fulfillment
of the requirements for the degree of
Masters of Science
2011

Advisory Committee:
Professor Gary Rubloff, Chair
Dr. Richard Cavicchi
Professor Michael Zachariah

DEDICATION

This thesis is dedicated to my wife Kelly and daughter Katelyn who have supported me throughout this long process as well as my parents James and Loretta who always encouraged creativity and curiosity while I was growing up.

ACKNOWLEDGEMENTS

This has been a long journey and of course there have been many people who have helped me along the way. I would first like to thank my advisor, Professor Gary Rubloff, who allowed me a great deal of flexibility in my project. It was his course that introduced me to the MSE department which I later joined as his student. While he is the busiest person I know, he always had time to help me when I ran into problems. Special thanks to my NIST co-advisor Dr. Richard Cavicchi for many discussions on bubble nucleation as well as helping me with the experiments and enduring the many proofreading sessions this work required. Thanks to Professor Michael Zachariah for taking time out of his hectic schedule to be on my committee. Of course none of this would be possible without the support of my past and current Division Chiefs and Group Leaders at NIST, Dr. James Whetstone, Dr. Michael Tarlov and Dr. Dean Ripple who always encouraged me in this endeavor.

On the technical side I would like to thank Professor Thomas Avedisian at Cornell for many conversations on this topic. He is an authority in the field of microboiling and his work on microbubble imaging is what got me interested in this area of research. Also, Christopher Montgomery for quite a few discussions on sputter deposition and general device processing and Dr. Kenneth Kreider, Dr. Weston Tew and Gregory Strouse of the NIST Thermometry Group for their vast knowledge of the properties of thin platinum films.

On the fabrication side, the staff at the Center for Nanoscale Science and Technology NanoFab at NIST, where all of the device fabrication was done, were invaluable for their assistance in this project. So thank you to the following individuals:

Dr. Gerard Henein for metal deposition. Marc Cangemi, Chester Knurek and Justin Dickinson for assistance with lithography. Jerry Bowser for developing and refining the low stress nitride recipe. Dr. Lei Chen for plasma etching help. Michael Hernandez and Richard Kasica for SEM and FIB assistance. Laurence Buck and William Young for helping me out with general equipment issues.

While this thesis is a major part of the program, there were also ten classes which needed to be completed to fulfill the degree as well. So I would like to thank the all of Professors in the MSE department who made their classes challenging and interesting.

On the administrative side, the staff at the graduate school office were extremely helpful and efficient at making sure I got through this process, especially when sudden deadlines appeared. And lastly, I do not know if anyone in the department would be able to get through this process without the help of our Assistant Director of Student Services Dr. Kathleen Hart. Without her support in navigating through the maze of forms and deadlines, I do not think I would have made it. No matter what issues came up (and there were quite a few), she was always able to resolve them quickly so thank you very much.

TABLE OF CONTENTS

DEDICATION ii

ACKNOWLEDGEMENTS iii

LIST OF FIGURES vii

LIST OF ABBREVIATIONS AND ACRONYMS x

Chapter 1: Introduction 1
- Previous Work 2
- Motivation 3

Chapter 2: Silicon Etching for Suspended Heaters 5
- Backside Etching 6
- Introduction to KOH Etching 8
- Wafer Selection 9
- Membrane Test Patterns – Scribe Lines 9
- ACES Tests 10
- Test Wafer Design 12
- Wafer Frontside Protection 13
- KOH Etch Rates 13
- Etched Test Wafer 14

Chapter 3: Device Design 16
- Device Layout 16
- Design Steps 17
- Device Layout 18
- The Final Masks 19

Chapter 4: Lithography 20
- Lift-off Process 20
- Cleaning After Lift-off 24

Chapter 5: Metal Deposition 25
- Choice of Metal 25
- Choice of Deposition Method 26
- Chamber Pressure 29
- Sputter Deposition 30
- Alignment of Substrate 32
- Shape of the Heater Lines 35

Chapter 6: Stress Management in Films 37
Metal Stress Measurement 37
Initial Stess Measurements 37
Stress vs. Temperature in Platinum 39
Annealing at 240 °C 41
A Final Test 41

Chapter 7: Fabrication 43
Process Steps 43
Device Inspection 44
Membrane Test 45
Temperature Coefficient of Resistance 46

Chapter 8: Packaging 47
Dicing 47
Dicing - Suspended Devices 47
Dicing - Non-Suspended Devices 48
Die Attachment 48
Die Attachment - Suspended Devices 48
Die Attachment - Non-Suspended Devices 48
Wire Bonding 51
Fluid Reservoirs 52

Chapter 9: Testing 54
Experimental Setup 54
6 μm Heaters - Water 56
4 μm Heaters - Water 57
2 μm Heaters - Water 58
2 μm Heaters - Ethanol 59
Discussion of Results 60

Chapter 10: Creation of Nanoscale Heaters 61
Design of Shielded Devices 64
Milling the Devices 66
Testing 68

Chapter 11: Conclusions and Future Work 70
Conclusions 70
New Applications 70
Future Work 70

REFERENCES 73

LIST OF FIGURES

Figure 1.1 – Detection of nucleation temperature from the heating inflection point 1
Figure 1.2 – Rise in nucleation temperature with increasing voltage................................ 2
Figure 1.3 – Bubble formation and collapse on a microsecond scale................................ 3

Figure 2.1 – NIST microhotplate gas sensor 5
Figure 2.2 – Comparison of space needed for backside etched membranes using DRIE (a) and with KOH (b). The membrane is shown on the bottom of each pit................ 6
Figure 2.3 – Diagram of KOH etch with a membrane width of zero (a) and with a width of m (b) 8
Figure 2.4 – Sample mask shapes 10
Figure 2.5 – 3D views of the top and bottom of the wafer 10
Figure 2.6 – Mask opening and result of etching for a square separated mask 11
Figure 2.7 – Mask opening and result of etching for finger pattern 11
Figure 2.8 – Mask opening and result of etching for refined finger pattern..................... 11
Figure 2.9 – Etch test mask. Region (a) contains scribe lines that go through the wafer Region (b) is the same but only goes ¾ through. Region (c) breaks the wafer into strips and region (d) contains many different corner configurations......................... 12
Figure 2.10 – Frontside protection wafer holder 13
Figure 2.11 – Silicon etch rates for various concentrations and temperatures of KOH ... 14
Figure 2.12 – Front and back of the etched silicon wafer showing membranes and scribe lines 14
Figure 2.13 – Images of the various etched corner patterns 15

Figure 3.1 – Basic design of a microboiling heater 16
Figure 3.2 – NIST four element microhotplate gas sensor design................................... 16
Figure 3.3 – Membrane size vs. etch pit mask opening with associated text 17
Figure 3.4 – Six element heater device mask design showing frontside metal mask superimposed on backside etch pit mask openings. The alignment mark design is on the right 18
Figure 3.5 – Six element microhotplate device mask design showing frontside metal mask superimposed on backside etch pit mask openings. An enlarged view of the heater is on the right.. 18
Figure 3.6 – Frontside and backside lithography masks superimposed over a 100 mm wafer outline 19

Figure 4.1 – Lift-off schematic 20
Figure 4.2 – SEM image of a lift-off profile of platinum showing incomplete removal of sidewall metal. The line width was 10 μm 21
Figure 4.3 – Cross section of developing lift-off photoresist 22
Figure 4.4 – Feature removal over a two minute period during development.................. 22
Figure 4.5 – SEM image of cross section of resist undercut 23
Figure 4.6 – AFM images of heater before and after cleaning 24

Figure 5.1 – Resistance change vs. temperature for selected metals 25
Figure 5.2 – Tensile stressed films 27
Figure 5.3 – Compressively stressed films 27
Figure 5.4 – Chamber pressure vs. flow over time 29
Figure 5.5 – Addition of an angled adapter to the sputtering system 30
Figure 5.6 – Overheated photoresist causes adhesion problems for the metal 30
Figure 5.7 – Target distance to the wafer using the adapter 31
Figure 5.8 – Inside of sputter chamber 31
Figure 5.9 – Thickness map of titanium deposition. The titanium is not aligned well..... 32
Figure 5.10 – Thickness map of titanium deposition. The alignment is better................ 32
Figure 5.11 – Perfectly aligned titanium deposition 33
Figure 5.12 – Three titanium depositions showing the effect of target rotation.............. 33
Figure 5.13 – Alignment of the chuck to the platen 34
Figure 5.14 – Final alignment of the platen 34
Figure 5.15 – AFM image of line made by lift-off with no undercut 35
Figure 5.16 – Effect of the Z-multiplier on the perception of the heater shape 35
Figure 5.17 – AFM profiles of the heater lines 36
Figure 5.18 – Percentage of height for each lines listed width 36

Figure 6.1 – Stress of a 100 Å titanium thin film vs. pressure 38
Figure 6.2 – Stress of a 2000 Å platinum thin film vs. pressure 38
Figure 6.3 – Annealing curve for 200 MPa film 39
Figure 6.4 – Second anneal showing initial anneal time was insufficient 39
Figure 6.5 – Anneals at various sputter pressures showing the stress differences 40
Figure 6.6 – An anneal to 240 °C did not change the film in the same way the 500 °C anneal did 41
Figure 6.7 – Metal misalignment and membrane destruction 41
Figure 6.8 – Glowing ribbon heater. The blue arrows indicate the current path 42
Figure 6.9 – The structure after heater failure. The remaining ribbon is still straight...... 42

Figure 7.1 – Completed bubble heaters on membranes 44
Figure 7.2 – Completed microhotplates on membranes 44
Figure 7.3 – Completed shielded nanoheater device 45
Figure 7.4 – Glowing microhotplate (a) and blown out membrane (b) 45
Figure 7.5 – Resistance vs. temperature for platinum heater 46

Figure 8.1 – KOH etched wafer showing the scribe lines on the back (a), the devices on the front of the wafer before separation (b) and the separated strips of devices (c) .. 48
Figure 8.2 – Schematic of the device mounting showing the device, spacer and package 49
Figure 8.3 – (a) The backside of the device showing the etch pits. The red line shows the edge of the front of the device, (b) The backside of the spacer. The red line shows the edges of the front of the spacer. (c) The spacer aligned with the device. The red line shows the attachment point 50
Figure 8.4 – 40 pin DIP package with 1 mm vent hole drilled in it, the spacer and the finished device ready to be assembled 51

Figure 8.5 – (a) Gold wire bonded to the device bond pad and (b) the DIP package pad 51
Figure 8.6 – Water beading on the device (a) and methanol conformally coating the surface of the package (b). It is not shown but the bottom surface is coated as well 52
Figure 8.7 – Uncut and cut plastic cuvettes 53
Figure 8.8 – The packaged device ready for testing 53

Figure 9.1 – Data acquisition circuit 54
Figure 9.2 – Bubble nucleation experiment setup 55
Figure 9.3 – Bubble nucleation in water for 6 μm heaters 56
Figure 9.4 – Bubble nucleation in water for 4 μm heaters 57
Figure 9.5 – Bubble nucleation in water for 2 μm heaters 58
Figure 9.6 – Bubble nucleation in ethanol for 2 μm heaters 59

Figure 10.1 – Creation of heater by removing all unwanted metal 61
Figure 10.2 – Creation of heater by electrically isolating the metal strip 61
Figure 10.3 – SEM image showing 345 nm heater 62
Figure 10.4 – SEM image showing massive charging 63
Figure 10.5 – The catastrophic result of a large arc due to charging 63
Figure 10.6 – LEdit drawing of the device showing the heater and ground links 64
Figure 10.7 – The actual fabricated device showing the heater and ground links 65
Figure 10.8 – SEM image of the 2 μm heater surrounded by and grounded to the metal shield. There was no visible charging at all 65
Figure 10.9 – SEM image of the first pass of the ion beam on the heater 66
Figure 10.10 – SEM images of some of the finished devices 66
Figure 10.11 – SEM image of cut ground link 67
Figure 10.12 – Cross sectional view of the layers in the heater 67
Figure 10.13 – Heater response vs. time for the 237 nm nanoheater 68
Figure 10.14 – Heater response vs. applied voltage at 1.9 μS showing an increase in resistance 69

Figure 11.1 – New low resistance heater design 71
Figure 11.2 – SnO_2 film grown on suspended heater 72

LIST OF ABBREVIATIONS AND ACRONYMS

ACES	Anisotropic Crystalline Etch Simulator
AFM	Atomic Force Microscope
CNST	Center for Nanoscale Science and Technology
DIP	Dual Inline Package
DRIE	Deep Reactive Ion Etch
DSP	Double Side Polished
FIB	Focused Ion Beam
KOH	Potassium Hydroxide
LPCVD	Low Pressure Chemical Vapor Deposition
NIST	National Institute of Standards and Technology
RIE	Reactive Ion Etcher
RTA	Rapid Thermal Annealer
SEM	Scanning Electron Microscope
SiN	Silicon Nitride
TEM	Transmission Electron Microscope
TCR	Temperature Coefficient of Resistance
ZIF	Zero Insertion Force

Chapter 1: Introduction

Microboiling heaters are currently used to measure the homogeneous nucleation of liquids. To measure the temperature of the homogeneous nucleation of a bubble, there is a need to bypass the nucleation occurring from an imperfection on the surface such as a pit or rough spot. To do this, the heat needs to be delivered extremely fast (microsecond pulse). The heaters used in these experiments are made from a metal whose resistance increases with temperature. As the voltage to the heaters is increased, the metal heats up and there is a rise in the slope of the signal which is dependent on the resistance of the heater changing. The system can be calibrated to convert the resistance to a temperature. This is represented in Figure 1.1 as the initial rise in the temperature [1]. When the heater reaches the nucleation temperature, a bubble forms in the liquid and there is now a vapor over the heater which is much less efficient at removing the heat and the temperature of the heater quickly rises with a different slope. The inflection point represents the nucleation temperature.

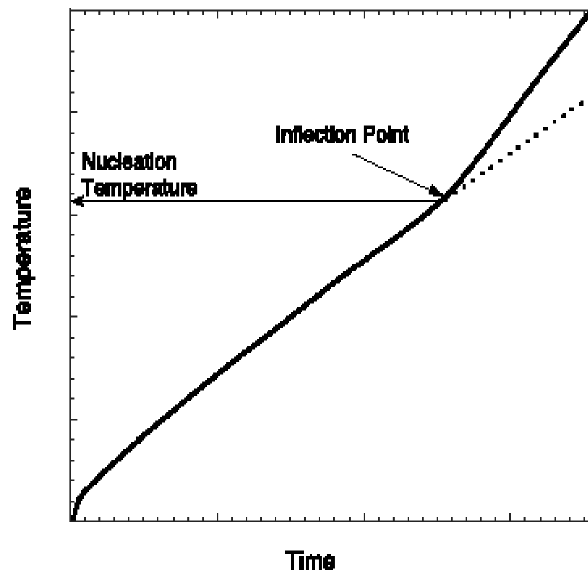

Figure 1.1 – Detection of nucleation temperature from the heating inflection point [1].

There have been questions as to whether or not bubbles formed by these heaters can be referred to as homogeneous nucleation since they are actually being formed on the surface of the heater and not in the bulk of the fluid. Experiments have shown that as the power to the heaters is increased, the nucleation temperature (determined by the inflection point) rises until it reaches a plateau which matches the theoretical homogeneous nucleation temperature of the fluid [1-3]. Figure 1.2 shows the increase in the nucleation temperature as the pulse voltage is increased [1]. Although the nucleation takes place on the heater surface, it is homogeneous in the sense that the bubble forms spontaneously in the fluid and not as a result of an expanding trapped vapor site on the heater surface. The heating rate of these pulses is on the order of 10^7 - 10^8 °C/s.

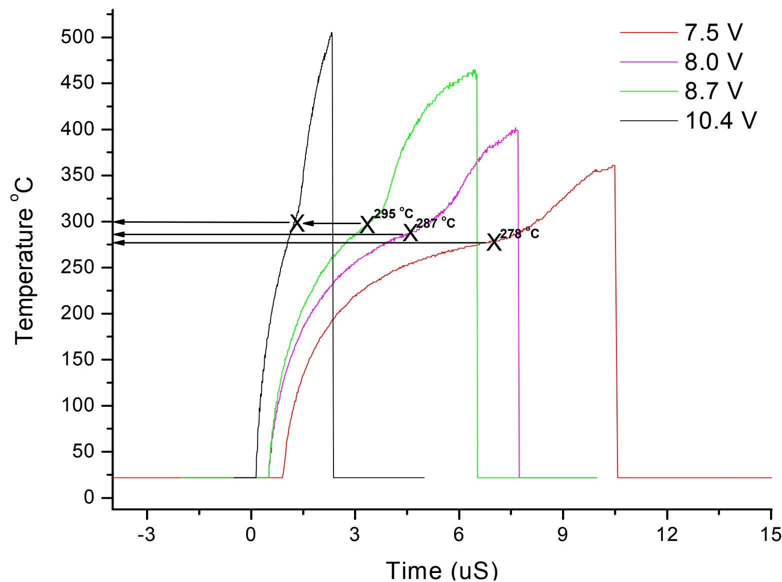

Figure 1.2 – Rise in nucleation temperature with increasing voltage [1].

Previous work

Microboiling has been studied for quite some time and in my research group at NIST from around 2002, but the heaters used have always been around 10 µm to 20 µm wide on non-suspended structures. This research follows the work done by Balss,

Cavicchi, Tarlov, Thomas and Avedisian [2] [4-6] on microbubble formation formed with ~5 μs voltage pulses. Their work was done on 15 μm wide heaters which were not suspended, meaning the silicon substrate is acting as a large heat sink. As will be shown in this work, the heat sink is responsible for higher required heating voltages and poorer signal quality compared to a device without this heatsink. The bulk of their work was on using the capability to image the extremely fast microbubble formation process [7] (Figure 1.3) using a pulsed laser as the illumination source to look at the properties of bubbles on different surfaces (Hydrophobic, Hydrophilic).

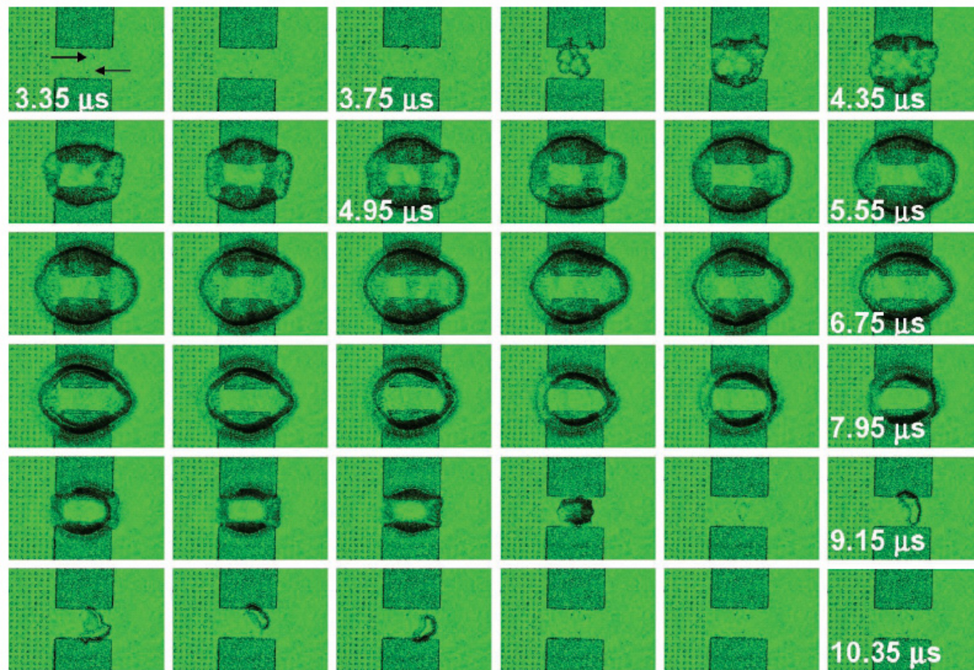

Figure 1.3 – Bubble formation and collapse on a microsecond scale [6].

Motivation

While current microboiling heaters work fine with water, they do not work quite as well with solvents. Since the thermal conductivity of the vapor is nearly the same as it is in the liquid, there is not a very large temperature change at the surface of the heater

during bubble formation and therefore the inflection point is very difficult to see. A thorough literature search turned up nothing related to increasing the sensitivity of microboiling experiments by using suspended platforms. Also, while suspended platforms have been used in sensor applications which involved heating, I was not able to find any work on their ability to hold up to the significant stress of bubble formation and collapse. By removing the heat loss through the substrate by using a suspended heater, I have shown that the signal from the nucleation event is greatly enhanced and allows the measurement of events that could not be seen using conventional non-suspended devices. Short pulse boiling is also important for inkjet printing [8] as well and without a substrate to absorb heat, boiling can be achieved at a lower power. This would be advantageous for portable printing devices as well as other devices where low power consumption would be advantageous such as MEMS bubble actuators etc. There was a study of the properties of fire suppressants done in my research group at NIST [9] which attempted to use the standard microboiling heaters in their experiments but since some of the suppressants were organic solvents or fluorocarbons, the heaters were not sensitive enough to see the inflection point at very short heat pulses. While the influence of the heater widths have been studied in the past by Deng, Lee and Cheng [10], they only looked at width to length ratios up to 1:3. This work looked at ratios ranging from 1:1 up to 1:20.

Chapter 2: Silicon Etching for Suspended Heaters

Suspending a heater can be done in many ways, the most common is to place it on a SiO_2 platform attached to the bulk silicon with thin arms and etch a pit down from the top to suspend it. This is the way the NIST microhotplate gas sensor devices are fabricated [11] (Figure 2.1). While this is a great design for gas sensors, it would not

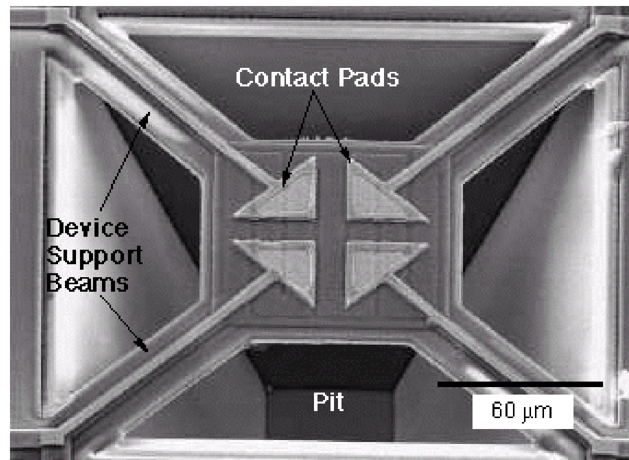

Figure 2.1 – NIST microhotplate gas sensor [11].

work well in microboiling experiments. Using this design, liquids would get inside the pit and the bubbles could form on both sides of the platform which is not desirable, especially if images are going to be taken of nucleation. Another common method of suspension is to deposit a layer of very thin (~2000Å) low stress silicon nitride (SiN) across the front of the wafer and etch completely through the wafer from the back, forming a membrane on the surface to suspend the heater. This completely isolates the back of the heater. A backside wafer aligner is required to place patterned heaters over these membranes as the patterns must be lined up on both the front and back of the wafer. The process engineers at the CNST Nanofabrication Facility at NIST have developed a LPCVD (Low Pressure Chemical Vapor Deposition) low stress SiN recipe which can form strong stable membranes up to 1 cm across.

Backside etching

There are two usual methods for etching through a silicon wafer, Deep Reactive Ion Etching (DRIE) [12] or wet chemical etching (usually KOH). The DRIE method is a plasma etch with alternating etch and polymer deposition steps to create a pit with very straight sidewalls. The wet chemical method etches the (100) crystal plane of the silicon fastest and the (111) plane slowest, forming an inverted pyramid when using a (100) wafer. The result of this is that the final opening in the surface of the wafer is quite a bit smaller than the mask opening depending on wafer thickness (Figure 2.2). This means that the individual heaters would need to be spaced further apart than those created with

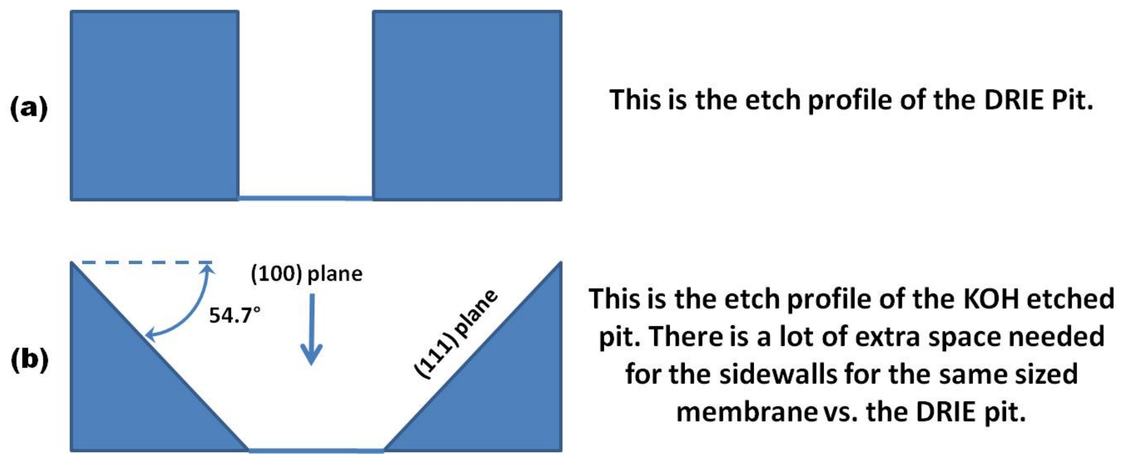

Figure 2.2 – Comparison of space needed for backside etched membranes using DRIE (a) and with KOH (b). The membrane is shown on the bottom of each pit.

DRIE so the etch pit openings on the backside did not overlap. The downside to DRIE however is that the wafer gets extremely hot during processing and needs to be cooled with pressurized liquid helium which can blow out the thin SiN membranes at the end of the etch. Also the DRIE process needs a thick photoresist layer to define the openings. The photoresist will be difficult to remove without damaging the membranes after they are released. The DRIE is also a much more expensive process than the KOH etch. I have listed the advantages and disadvantages of both methods below.

DRIE:

Advantages

Faster Etch (Two Hours instead of six for a 500 µm thick wafer).

Can position etch pits closer together and get more per die.

Disadvantages

Cost is $63/Hr in the CNST NanoFab.

Need to clean off baked photoresist from the back.

Cooling gas can blow out membranes at the end of etching.

Complicated tool – Long repair time if something breaks.

Somewhat heavily used.

KOH Etch:

Advantages

Free

Backside etch mask is made from the existing SiN layer on the back.

Overetching only makes the membranes slightly larger.

Simple system – A KOH change is all the maintenance required.

Not used as often as DRIE.

Disadvantages

Slower etch.

Features need to be farther apart.

After reviewing the list above, the KOH etching was chosen to create the membranes.

Introduction to KOH Etching

As was seen in the section above, a KOH etch gives a triangular pit with a 54.74° angle to the surface. Figure 2.3(a) shows the triangular etch pit as it just touches the front

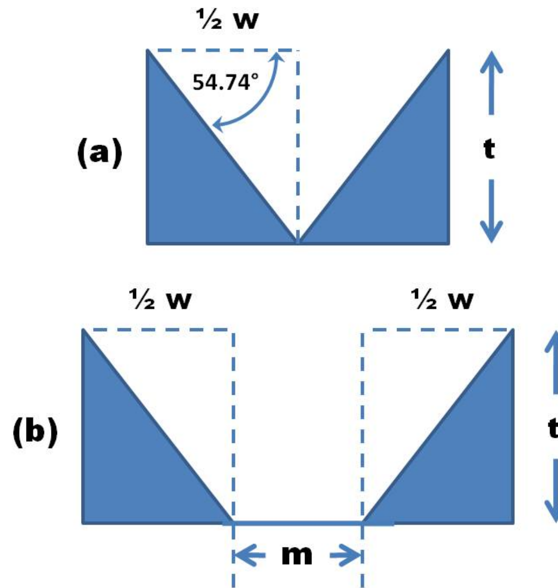

Figure 2.3 – Diagram of KOH etch with a membrane width of zero (a) and with a width of m (b).

side of the wafer. Solving for ½ **w** where **t** is the thickness of the wafer, gives Equation 2.1 which gives the width of the backside mask for a membrane size of zero. This is

$$^{1}/_{2}\ w = t\ /\tan(54.74) \tag{2.1}$$

essentially the minimum opening size needed and for a 500 µm wafer it is 709 µm. Any increase in the mask opening gives an identical increase in the membrane size. The final formula for the mask opening is shown in Equation 2.2. Note that unless wafers

$$Mask\ Opening = 2 * (t/\tan\,(54.74))\ +\ m \tag{2.2}$$

with very tight thickness uniformity (expensive) are purchased, the mask needs to be designed to work with the thickest wafer of the batch. Thinner wafers will give a larger membrane but that is much better than it being too small and not going across the entire heater or worse, having to design and fabricate many masks.

Wafer Selection

The wafers which I have used in the past to fabricate sensors have been single side polished test grade wafers with no thickness uniformity between them. While this is acceptable if the wafer is just a platform, it is not good for backside etched devices for the following reasons:

1. The etch opening will give a membrane size depending on the thickness of the wafer. Thicker wafers will result in smaller membranes while thinner ones give larger ones for a given mask. As a result, a narrow thickness range is needed or extra masks will be required to keep the membrane size within the desired range.
2. For etching to work correctly, the wafer needs to be <100>.
3. The wafer needs to be double side polished (DSP) to allow for uniform etching. This is not a problem with large membranes in the millimeter scale but it is for 100-200 μm membranes. The roughness on the back of a single side polished wafer also requires the use of very thick photoresist which is harder to work with than commonly used thin photoresists such as Shipley 1813.

Therefore, in this work, <100> double side polished wafers with 25 μm uniformity were used.

Membrane Test Patterns – Scribe Lines

With non-suspended devices, a dicing saw is used to separate the die. With devices containing membranes however, this method does not work so well. Even if the vibrations form the saw did not destroy the membranes, the water spray that cools the wafer and washes away the particles would. The solution to this is to etch scribe lines between the devices so they can be easily broken apart after etching. There is a trade-off

in the design, the scribe lines should make separating the die easy but not weaken the wafer to the point where there is a risk that it might fall apart during etching.

ACES Tests

ACES, is the Anisotropic Crystalline Etch Simulator developed at the University of Illinois to simulate silicon etching [13]. This software provided a 3D picture of silicon etching of different wafer orientations and surfaces. It was used for the design of the connections between the die so the wafer will not fall apart during etching. This was needed because silicon wet etch mask design is not as simple as with plasma etching. A circle and square mask opening will give the same etch result (square). The program uses a bitmap file to represent the mask openings which can be made by any drawing program. In wizard mode, the program brings up Microsoft Paint to create the mask. My first test was a few simple shapes as shown in Figure 2.4. Figure 2.5 shows the results

Figure 2.4 – Sample mask shapes.

after 200 minutes of etching were simulated. A nice feature of this program is that it provides a 3D view and the ability to rotate the image as well. The rectangle etched part

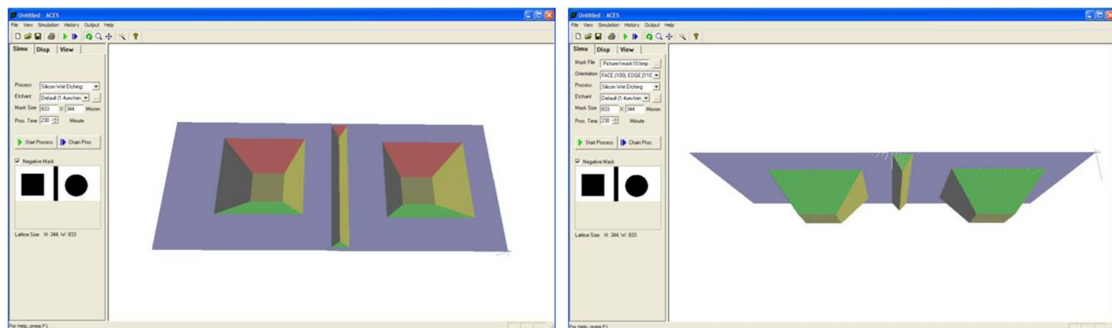

Figure 2.5 – 3D views of the top and bottom of the wafer.

of the way through the wafer made a nice scribe line.

Now there were many different line patterns simulated to get an optimal corner. Figure 2.6 shows separating the lines with a square to get inverted pyramid as the corner

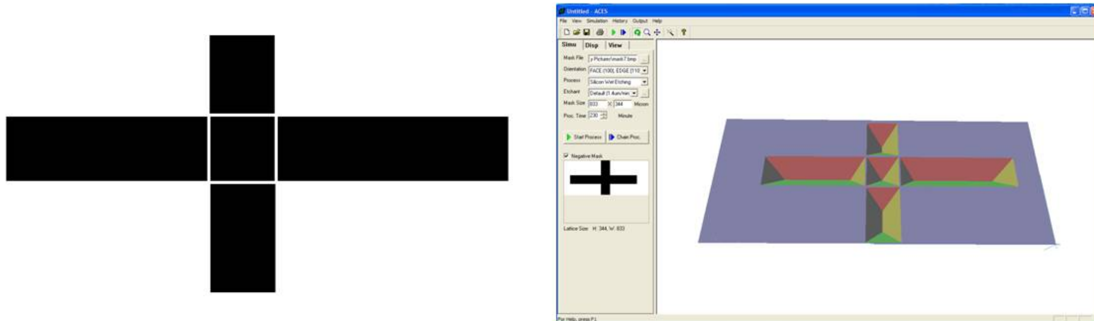

Figure 2.6 – Mask opening and result of etching for a square separated mask.

between the die. Figure 2.7 uses small fingers that slightly overlap each other such that at some point in the etch, the pits will start to overlap and connect with each other. Figure 2.8 is an enhancement on the fingers which keep the corners more square. In this simulation the actual overlap does not take place until after 125 minutes.

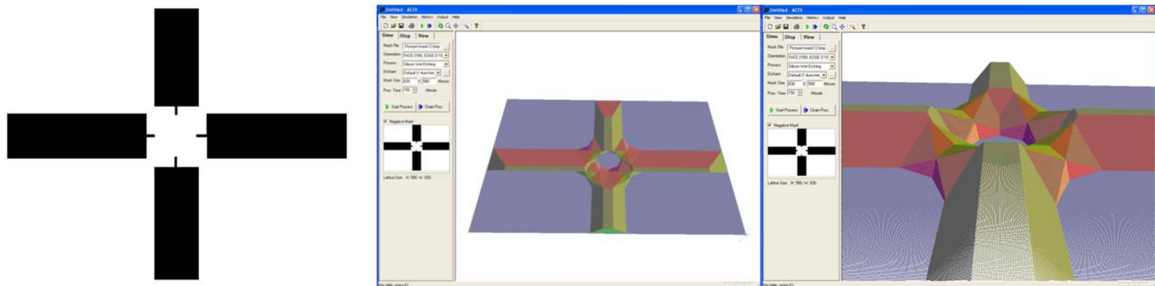

Figure 2.7 – Mask opening and result of etching for finger pattern.

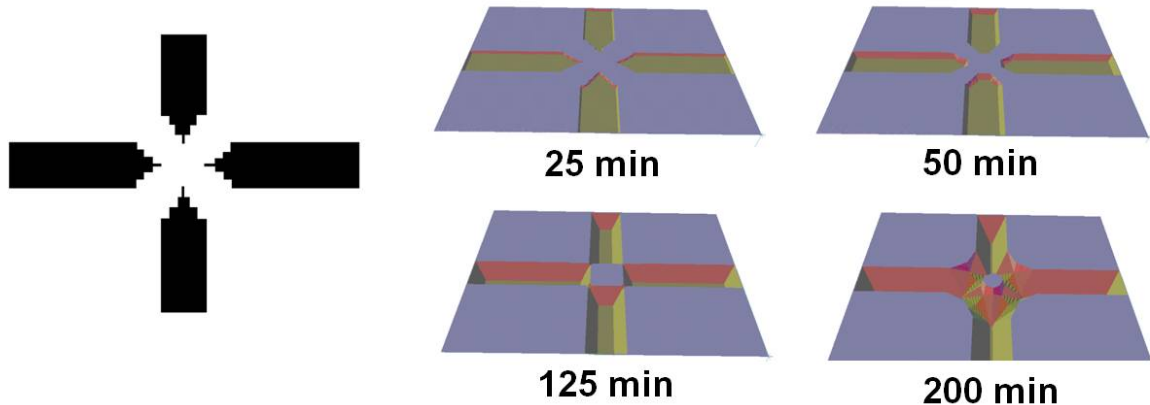

Figure 2.8 – Mask opening and result of etching for refined finger pattern.

Test Device Wafer Design

Figure 2.9 is a schematic of the wafer designed to test the membrane fabrication and the etched scribe lines to see which gave the best results. The scribe lines used many different corner combinations and depths while the membranes widths ranged from 100 μm to 3 mm.

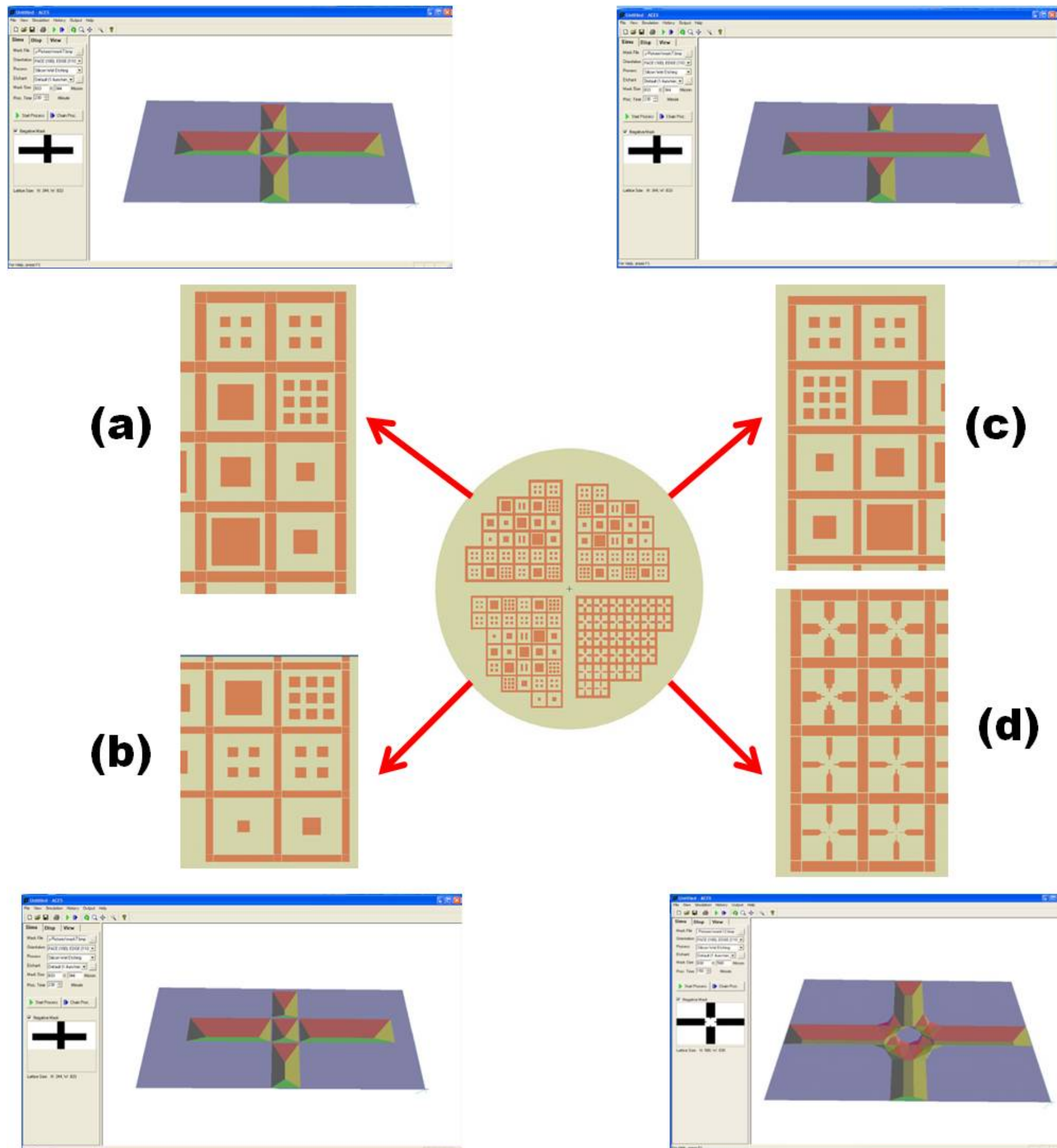

Figure 2.9 – Etch test mask. Region (a) contains scribe lines that go through the wafer. Region (b) is the same but only goes ¾ through. Region (c) breaks the wafer into strips and region (d) contains many different corner configurations.

Wafer Frontside Protection

Because the platinum and titanium cannot stand up to the KOH etch for the many hours needed to etch through the silicon or the HCl cleaning step, a special protective wafer holder is used for the etch [14]. The holder, shown in Figure 2.10, from Advanced Micromachining Tools, is made from a chemical resistant material and uses multiple O-rings to keep etch chemicals from reaching the front side of the wafer during the etch. There is also a vent tube so there is not a pressure differential behind the wafer when a heated bath is used. This worked quite well for these devices with the only drawback being that it was much harder to see the released membranes than it was when they were in a wafer boat and light could shine through them. There are some manufacturers that make these holders with LED lighting in the back but they are quite expensive.

Figure 2.10 – Frontside protection wafer holder [14].

KOH Etch Rates

KOH etching is a nonintuitive process in that the etch rate goes down as the concentration increases. The surface roughness is also dependent on the etch rate with the sidewalls becoming rough once the concentration drops below 30%. One issue in a long

etch is that if the solution is not mixed, a concentration gradient can occur and a non-uniform etch could occur. Temperature is also an important factor in the etch rate and Figure 2.11 shows the effects of temperature and concentrations on the etch rates [15].

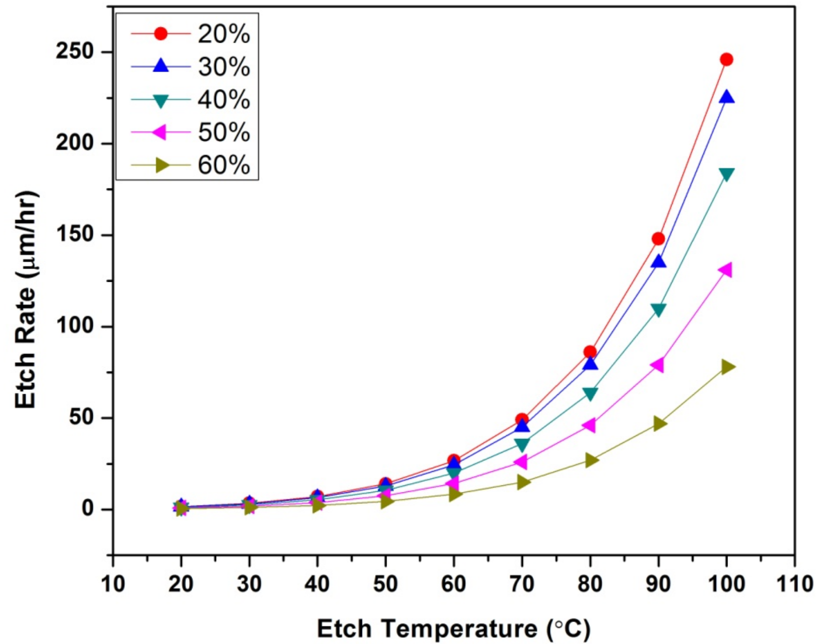

Figure 2.11 – Silicon etch rates for various concentrations and temperatures of KOH [15].

Etched Test Wafer

The result of the etch is shown in Figure 2.12. The protection fixture was not used for this etch as it was desired to see exactly when the membranes opened up. Only two of the 1.5 mm membranes failed during etching while the rest survived intact.

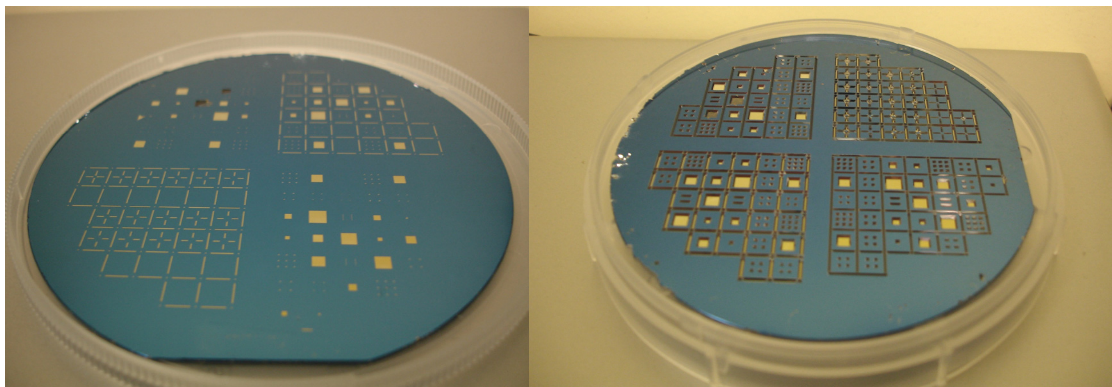

Figure 2.12 – Front and back of the etched silicon wafer showing membranes and scribe lines.

The results of the corner etch structures are shown in Figure 2.13. When separating the die, the corner given by 2.13(d) separated the best and gave the least corner damage. The large (3mm) membrane devices broke apart if the scribe line did not go through the wafer. A test in the protection fixture however gave completely different results. There was massive overetching of the corners of the lines that went completely through the wafer and a lot of the die fell into the solution. The only difference is that the fixture is held higher in the etch bath where the KOH concentration is lower towards the end of the etch cycle and it may also keep the solution from circulating. In this case, the one that worked best for the small membranes used with these devices was 2.13(p). The 3 mm membrane devices which will be used as spacers in the mounting of the devices did not need the protection fixture and they will be made with the Figure 2.13(d) pattern.

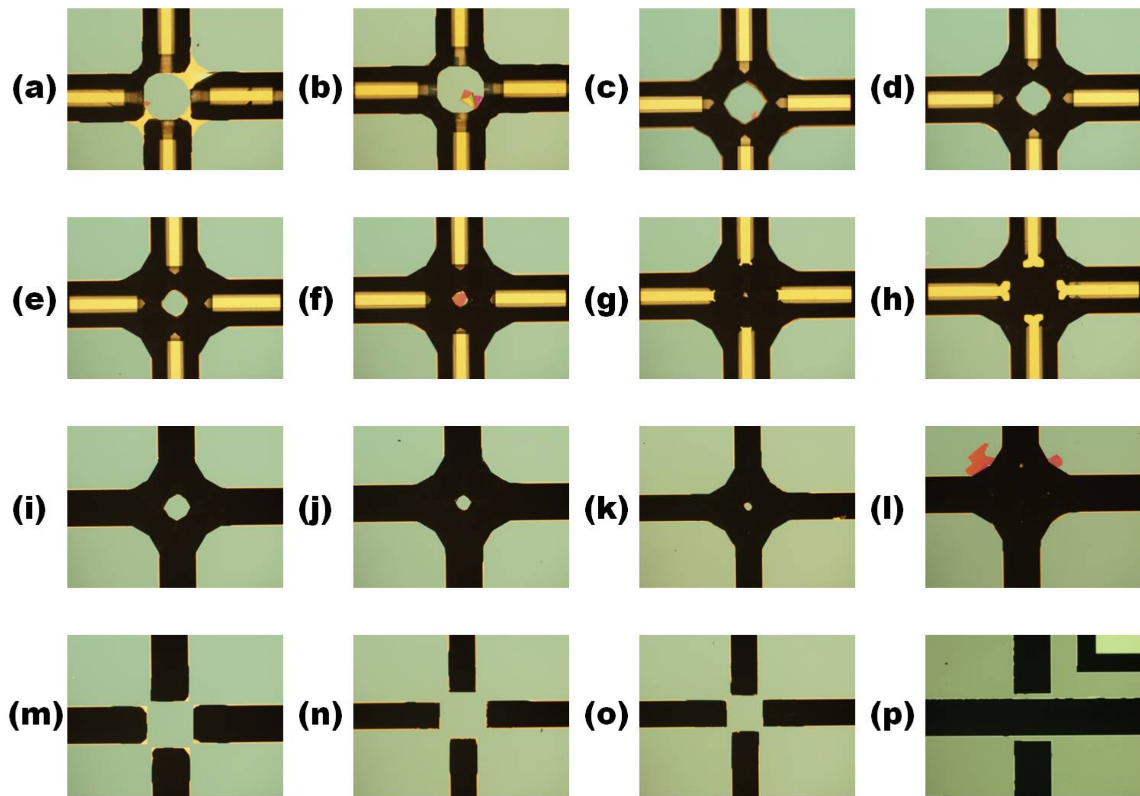

Figure 2.13 – Images of the various etched corner patterns.

Chapter 3: Device Design

The basic design of a microboiling heater is shown in Figure 3.1. The tapered design has been shown to increase the lifetime of the heater as sharp corners were usually the sites of heater failure in previous devices. A heater is characterized by both its

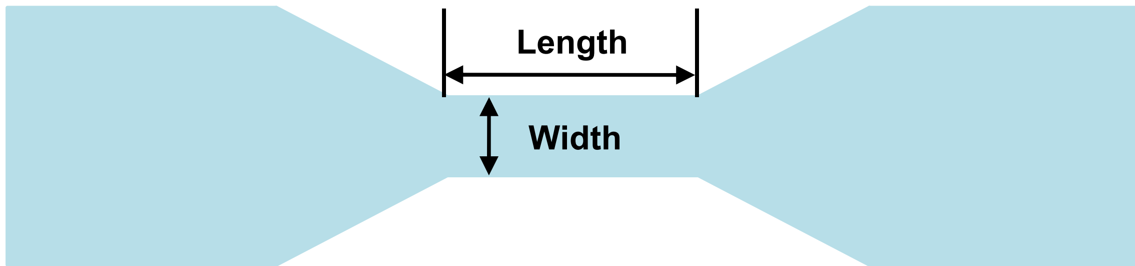

Figure 3.1 – Basic design of a microboiling heater.

width and the width/length ratio. A 2 μm wide heater that is 20 μm long would be referred to as a 2 μm, 1:10 heater. This is how the devices will be referred to throughout this document.

Device Layout

The layout of the device is based on a multi-platform gas sensor device designed for my research group at NIST. It consists of bond pads on the outer edges and the sensors equally dispersed throughout the die and is shown in Figure 3.2.

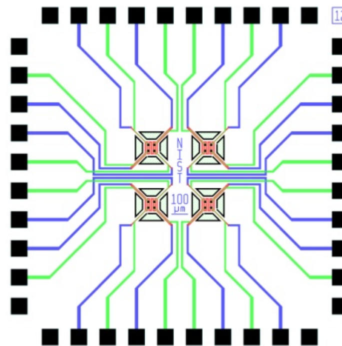

Figure 3.2 – NIST four element microhotplate gas sensor design.

Design Steps

The die size was the limiting factor for the number of devices per die. The die is 5 mm (5000 µm) on a side to allow it to be mounted in a 40 pin package. Using the etch pit data, the extra space required per device is 740 µm for a 525 µm thick wafer. An 890 µm backside opening is required to create a 150 µm membrane. A top view layout is shown in Figure 3.3. The purple area is the actual membrane and the red area is the mask

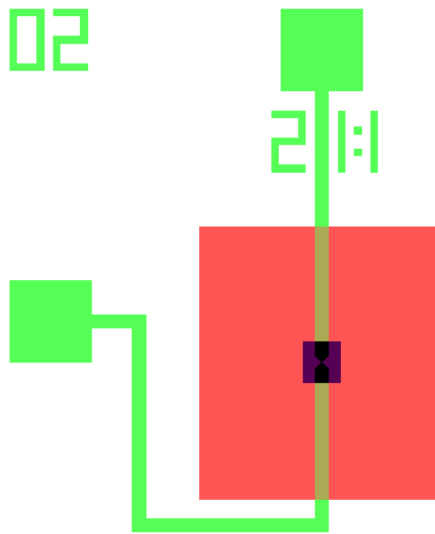

Figure 3.3 – Membrane size vs. etch pit mask opening with associated text.

opening on the back of the wafer. The pits should be sufficiently far enough away from the bond pads that there is no chance of undercut and die damage during wire bonding step. Another important feature of sensor design is to place labels on each die and individual device which can be seen with a magnifying glass. Figure 3.3 shows the die label in the top left and the heater identifier. A text height of 250 µm is all that is required for it to be seen. Another important consideration is the dicing. These devices were designed to allow the possibility of both dicing by KOH etching for the suspended device configuration or the mechanical dicer for the non-suspended configuration.

Device Layout

Figure 3.4 shows the completed design for the heaters as well as the backside alignment marks. Figure 3.5 shows the design for the microhotplate heaters which will be

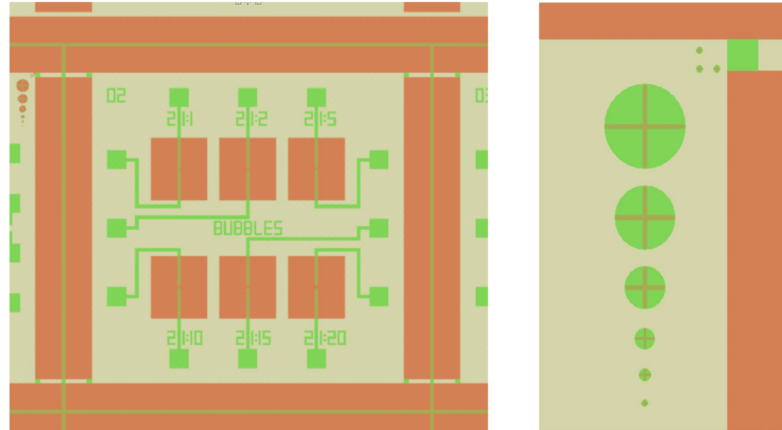

Figure 3.4 – Six element heater device mask design showing frontside metal mask superimposed on backside etch pit mask openings. The alignment mark design is on the right.

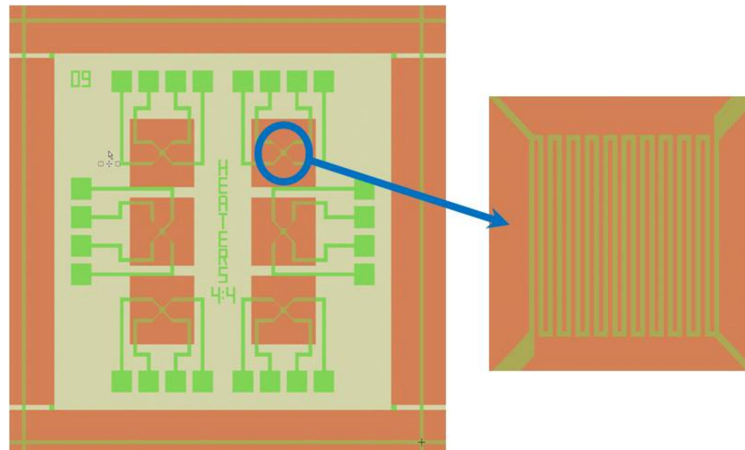

Figure 3.5 – Six element microhotplate device mask design showing frontside metal mask superimposed on backside etch pit mask openings. An enlarged view of the heater is on the right.

used to test the membranes as well as determine the TCR of the platinum. The red is the backside mask openings for the KOH etch for both the membrane pits and dicing lines. Also surrounding each die are thin metal lines which were used to assist in lining up the manual dicer blade.

The Final Masks

Figure 3.6 shows the overlay of the heater mask and the backside etch mask superimposed over a four inch wafer. The areas which appear solid green are the devices which were made into nanoheaters and those are described in Chapter 10. There is a row of blank die on the top and bottom of the wafer to allow for the snapping off of the top and bottom wafer pieces without damaging the devices.

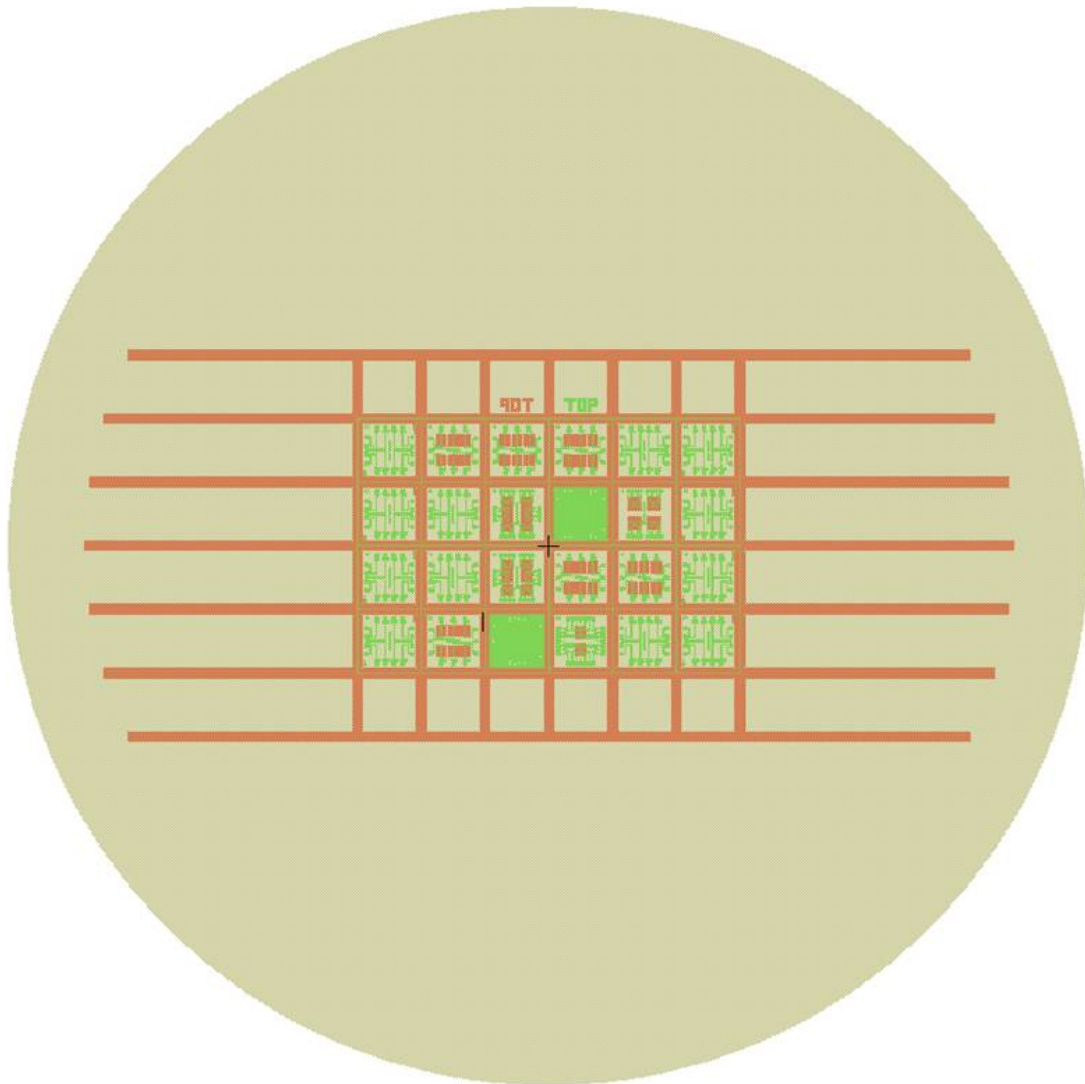

Figure 3.6 – Frontside and backside lithography masks superimposed over a 100 mm wafer outline.

Chapter 4: Lithography

While lithography seemingly is the most standardized process out of all of the fabrication steps, there were still issues to be confronted. As with most other processes, listed parameters are only guidelines and designed for commercial fabrication facilities with more advanced resist processing equipment than at a research facility. Therefore process optimization needed to be done before metal deposition could proceed. I developed a novel method to characterize the lift-off undercut without the use of an SEM.

Lift-off Process

The two methods of lift-off commonly used are shown in Figure 4.1. Using a single layer lift-off or a bi-layer method that did not produce an undercut yields the result

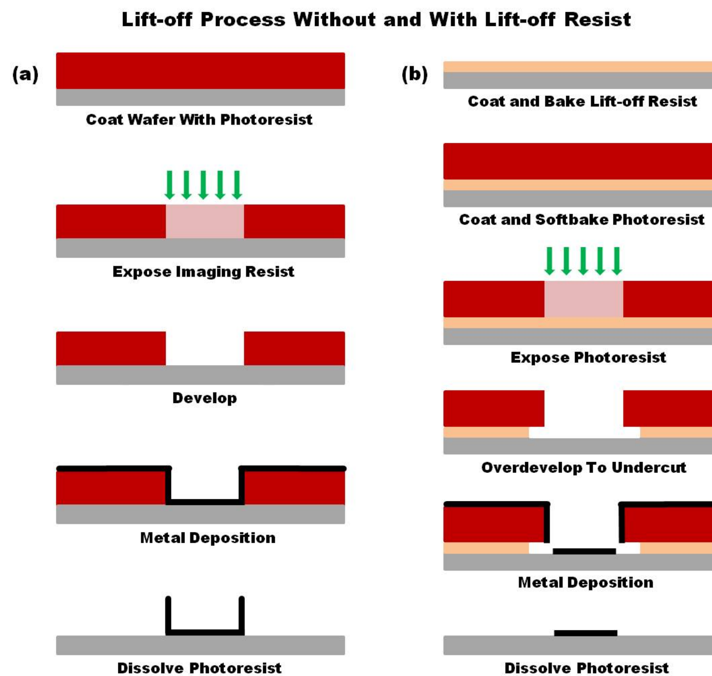

Figure 4.1 – Lift-off schematic.

in Figure 4.1(a) which gives lines with tabs or "ears" on the edges. A better method is to use a thin layer of lift-off resist [16] which is not photosensitive as the first layer and coat that with the standard photosensitive layer. During development the top layer features

develop where they were exposed to UV and then the bottom feature dissolves at a rate dependent on how long it was baked as shown in Figure 4.1(b). If it was timed right there would be an undercut and the sidewalls are not connected to the bottom. The tricky part is how to determine the undercut. Too much and the top layer of resist collapses and too little and the metal coating the sidewalls will be continuous to the substrate. The first attempt at lift-off was done using the listed LOR bake temperature of 200 °C. The result, shown in Figure 4.2 shows that there is residual metal left behind at the edges. This

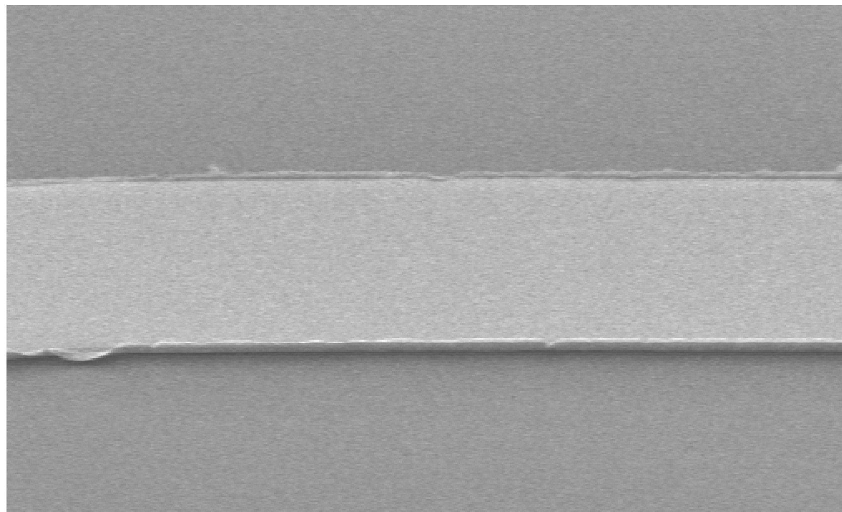

Figure 4.2 – SEM image of a lift-off profile of platinum showing incomplete removal of sidewall metal. The line width was 10 μm.

implies that there was little or no undercut. This meant that some process optimization [17] needed to be done before metal deposition could proceed.

It was necessary to have a method for characterizing the lift-off process. The standard method for profiling lift-off is to run a set of patterning steps and then break the wafer and look at it edgewise in a SEM to get a profile. Considering that the SEM is reserved quite often, I sought another way to profile the undercut. A narrow opening will have smaller undercut than a wide opening when doing a manual develop (spray development does not suffer from this) due to developer not getting recirculated in the

thin channels. Given a set of parallel lines of a given width and an undercut distance of one half the width or more, the feature will come off as shown in Figure 4.3. Therefore a small mask with many groups of parallel lines of different widths separated by different gaps will tell me whether the lift-off is creating the proper undercut. When establishing the process parameters it is important that the undercut not happen too fast or there will

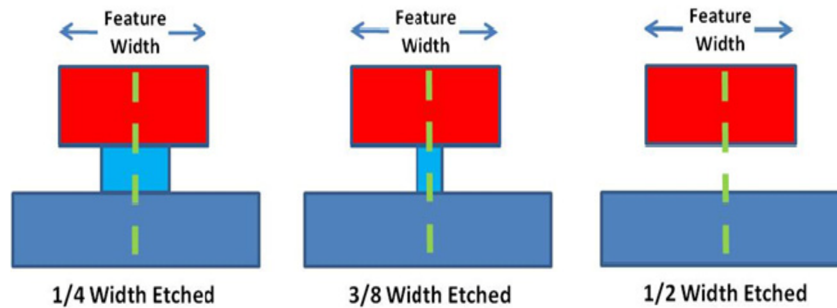

Figure 4.3 – Cross section of developing lift-off photoresist.

be a loss of control, however too slow is bad as well because the top layer will be overdeveloped. After many iterations I found that a lift-off resist bake of 5 minutes at 170 °C gave the best results. Figure 4.4 shows the development results of three of the

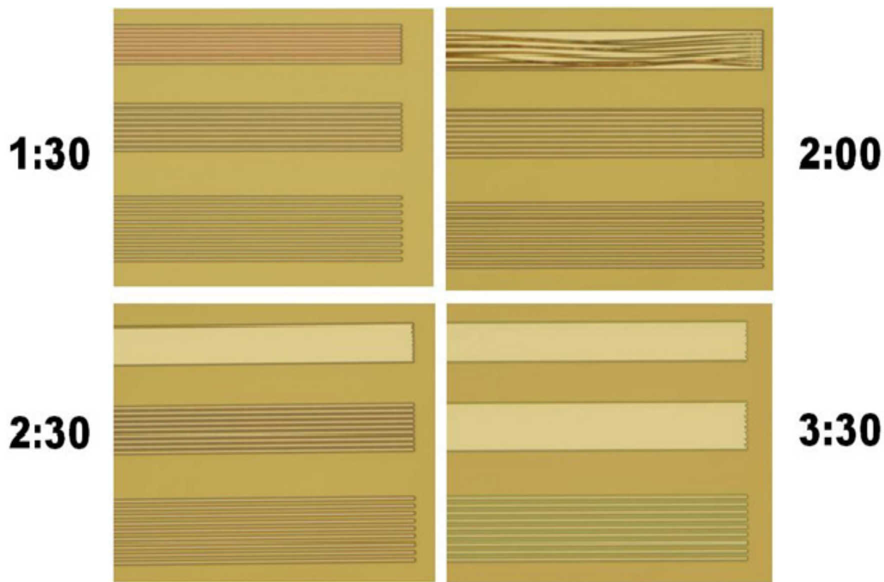

Figure 4.4 – Feature removal over a two minute period during development.

many sets of lines on the test feature. The openings are all 2 μm and the line widths are 2 μm, 3 μm and 4 μm from top to bottom. At 1.5 minutes in the development, everything is fine and the undercut has not resulted in released features. At 2.0 minutes, the 2 μm features are starting to come off meaning the undercut is getting close to 1 μm on each side. By 2.5 minutes they are gone and at 3.5 minutes the 3 μm features are gone as well. Since none of my features are 2 μm or less, I can use the 2.5 minute development and get between a 1 μm and 1.5 μm undercut. Now the SEM can be used a single time to check how well this method works. Looking at the cross section in Figure 4.5, the undercut is 1.304 μm which is exactly what was predicted by this method. It turns out that the development technique is quite uniform as the larger openings had the same undercut as the smaller ones.

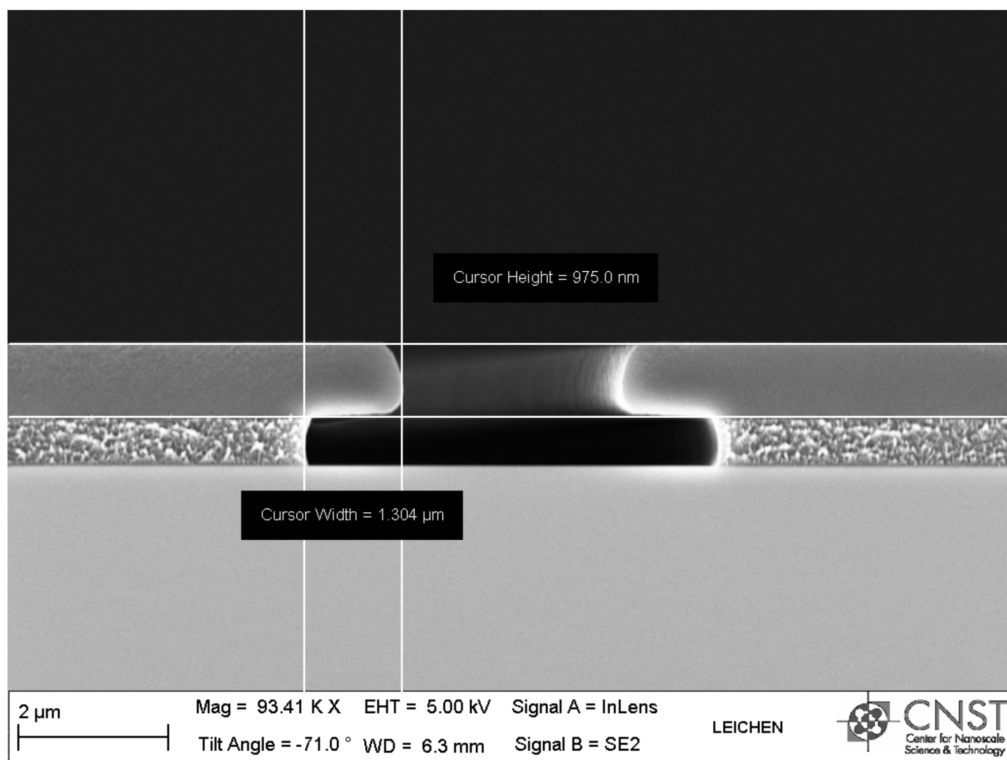

Figure 4.5 – SEM image of cross section of resist undercut.

Cleaning After Lift-off

Lift-off is quite a dirty process. While it looks like the metal is coming off in sheets, there are actually many small metal particles coming off of the sidewalls which attach themselves to the metal features. While this might not be a problem for some devices, these particles could be bubble nucleation sites which would affect the heater performance. The figures below show the AFM scans before and after cleaning of the platinum heater. While Figure 4.6 shows a lot of particles on the leftmost image, it was actually taken after the device was cleaned with solvent and q-tips. The only way to get them completely clean is to use a cleaning solution consisting of Sparkleen which is a lab glassware detergent (surfactant) in a mixture of 75% ethanol, 23% 1165 Remover and 2% acetone [18].

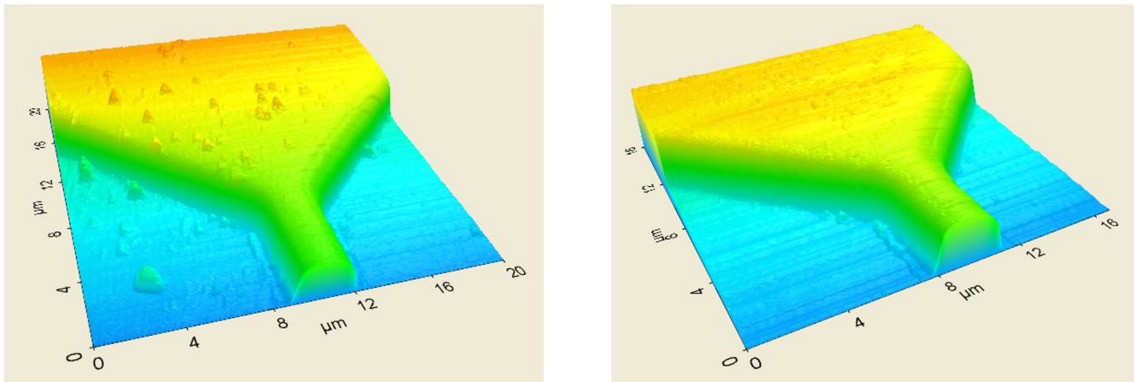

Figure 4.6 – AFM images of heater before and after cleaning.

Chapter 5: Metal Deposition

The metal selection and deposition method for the heaters is described in this chapter. While this was initially thought to be an easy part of the project, it turned out to be more complicated than originally anticipated due to the stress minimization aspect.

Choice of Metal

There are three criteria to look at in the choice of the heater metal.

1. The resistance needs to vary with temperature because the heater also acts as a thermometer to measure the nucleation temperature
2. The metal needs to be hard.
3. The metal needs to be stable in water and atmosphere at high temperature.

Some of the metals initially considered were Nickel, Gold, Platinum, Nichrome and Tungsten. While nichrome is hard and inert, its resistance does not vary with temperature (which is why it is used in resistors). Looking at Figure 5.1, the resistance change of nickel is non linear which makes it unsuitable as a thermometer. Of the remaining three,

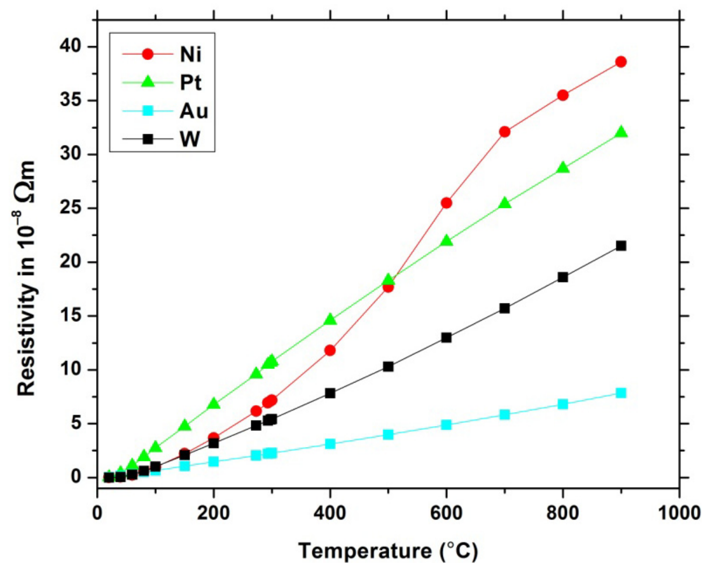

Figure 5.1 – Resistance change vs. temperature for selected metals [19].

the resistance slopes are all linear but tungsten oxidizes too easily at high temperatures. Gold has been used in the past for microboiling experiments [5] and while it gives an acceptable signal, it was found to erode under repeated cycles of bubble formation and collapse. Platinum is very hard and has a nearly linear Temperature Coefficient of Resistance (TCR) which makes it ideal for the heater metal.

Choice of Deposition Method

One of the major choices that had to be made in this project is how to put down the platinum for the heaters. The CNST Nanofabrication Facility at NIST has both a Magnetron sputtering and e-beam evaporation system for metal deposition. There were two things to take into account when choosing the deposition method.

1. Since the metal features will be on suspended structures, the stress control is very important. This is especially true at the endpoint of the etch process when the membranes are released from the silicon. If the metal stress is too great the membrane could be destroyed by the now released stressed metal films.
2. The patterning of the platinum requires lift-off.

The standard recipes in our facility are not optimized for stress (with the exception of the low-stress SiN) therefore I needed to optimize the process myself. Since either method of deposition will require modification of the standard recipe the question arose as to which method will work best. Figures 5.2 and 5.3 [20] show the benchmark stresses measured by the process engineers at our facility. All of the metal films are deposited at the same pressure if sputtered (3.2 mTorr).

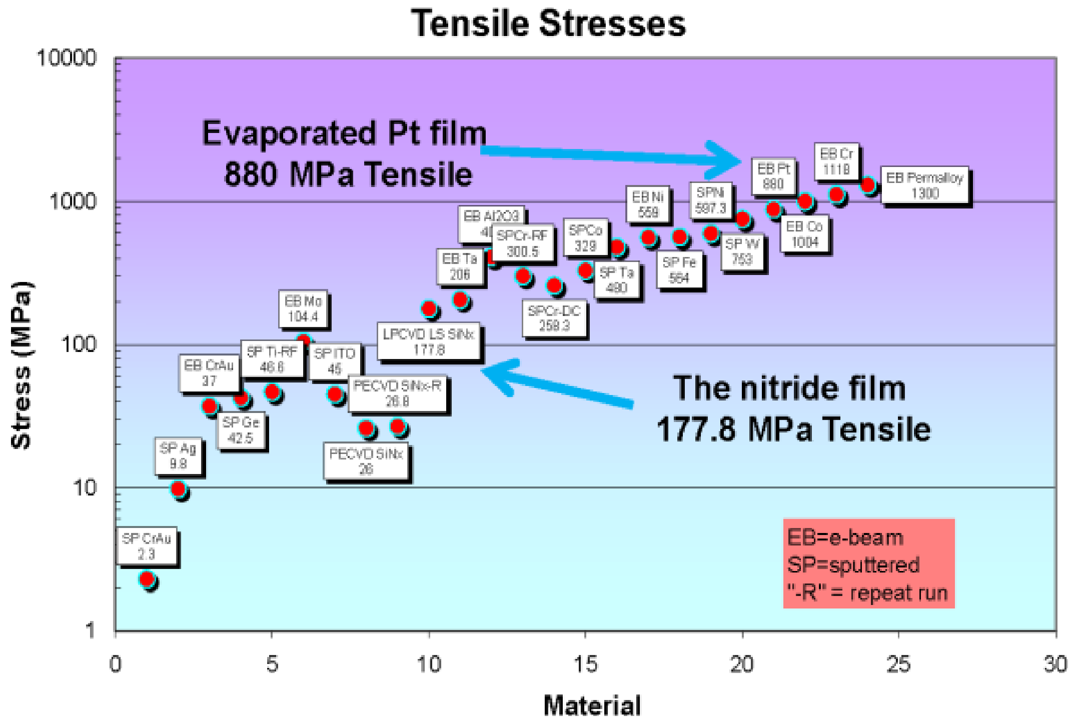

Figure 5.2 – Tensile stressed films [20].

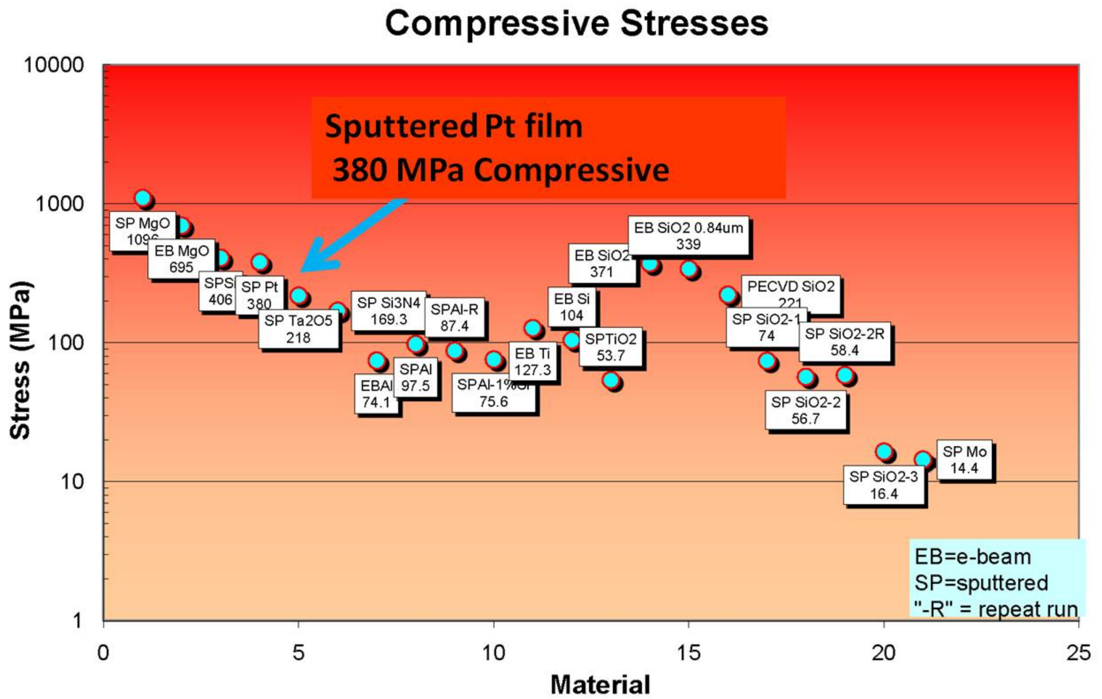

Figure 5.3 – Compressively stressed films [20].

The advantages and disadvantages of the two methods are as follows:

Evaporation Advantages

Ideal for Lift-off

Very good uniformity across wafer

Evaporation Disadvantages

Difficult to get a lot of time to optimize the process

1-2 week wait for a time slot of two hours (one of the most heavily reserved tools).

Takes a long time per wafer (very long chamber pump down).

Uses a lot of platinum – (Fine for multi-wafer runs but wasteful for single runs).

Limited amount of platinum in CNST NanoFab Evaporator

Sputtering Advantages

Easy to get time on the tool.

Can do a single wafer in 40 minutes.

Stress is adjusted by varying the deposition pressure.

New platinum target for CNST NanoFab sputter tool.

Uses much less platinum per run than the evaporator.

Sputtering Disadvantages

Not currently setup to do lift-off.

Uniformity is not as good across the wafer as evaporated films.

Sputtering was chosen for the metal deposition. The main factor in this decision was the availability of the tool and quick turnaround for a single wafer. The original estimate of

20 wafers to characterize the films grew much larger by the time the project was finished so there would not been enough available time on the evaporator. Also, depleting the evaporator platinum supply would not have gone over well.

Chamber Pressure

The sputter pressure for the deposition tool is set by using a mass flow controller to provide a fixed argon flow into the chamber to achieve a particular sputter pressure not by a pressure feedback system. The pressure however does remain constant throughout the deposition. Since the stress in the metals is altered significantly by very small changes in the pressure it was important to look at the stability of the chamber over time which is shown in Figure 5.4.

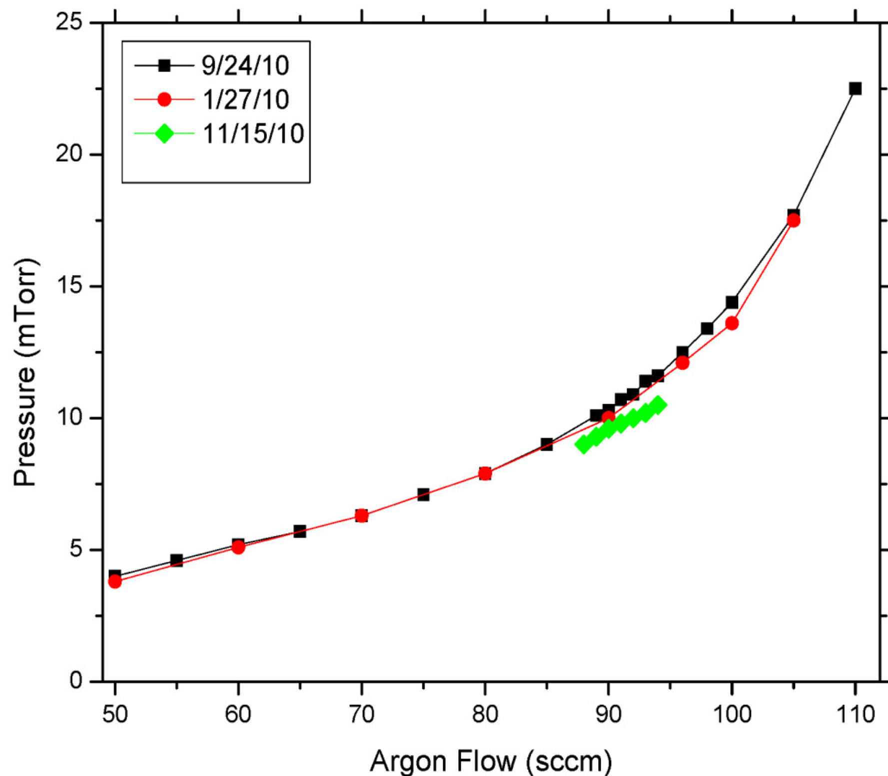

Figure 5.4 – Chamber pressure vs. flow over time.

Sputter Deposition

In most sputter chambers, the guns are at an angle to the rotating substrate to get a uniform film deposition. This method does not work well with a lift-off process as the photoresist blocks the metal path and very small features do not come out well. While some tools have guns that can line up with the wafer, an adapter was needed to angle the wafer (Figure 5.5). The first test was a disaster as the photoresist overheated and wrinkled as the metal deposited as shown in Figure 5.6. Lowering the power did not

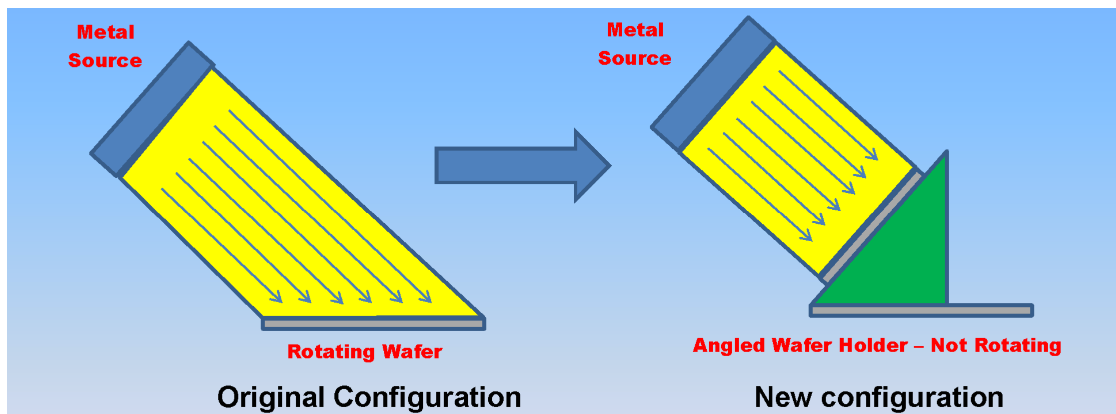

Figure 5.5 – Addition of an angled adapter to the sputtering system.

Figure 5.6 – Overheated photoresist causes adhesion problems for the metal.

really help but modifying the adapter distances did. Figure 5.7 shows a before and after visualization of the process used with the dimensions added. Adding the adapter reduced the sputter distance from the optimal 12 cm [21] by 4.5 cm and as the substrate is not

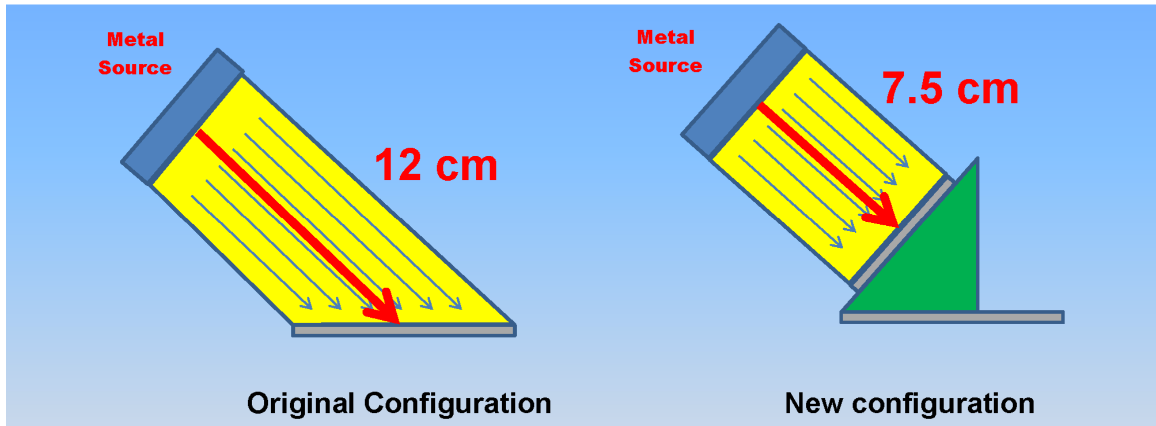

Figure 5.7 – Target distance to the wafer using the adapter.

rotating, there was a large heat buildup resulting in damaged photoresist. Fortunately the tool was designed with adjustable guns and when the target was moved back so the distance was 12 cm to the wafer, the problem was solved. Figure 5.8 shows a picture of the inside of the chamber with the adapter and pulled back guns.

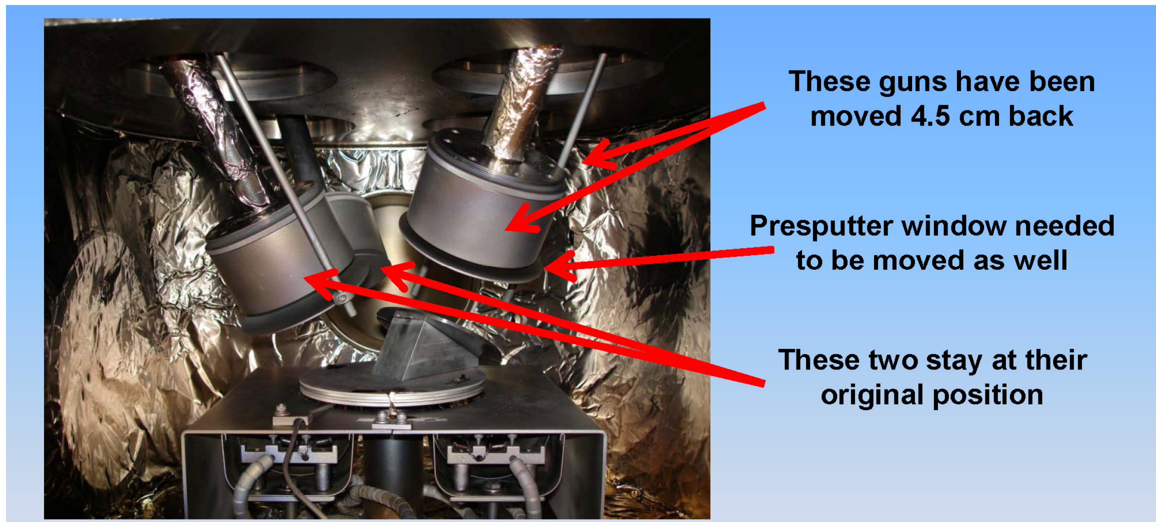

Figure 5.8 – Inside of sputter chamber.

Alignment of Substrate

The alignment of the wafer to the guns was the next step. This did involve some trial and error to get the alignment correct. Since the thickness of a thin layer of titanium (10 nm) is able to be measured by a scanning ellipsometer, I was able to get a map of the metal thickness across the wafer and from that know how to do an alignment of the chuck. Figure 5.9 shows the thickness map of the sputtered titanium and it looked like

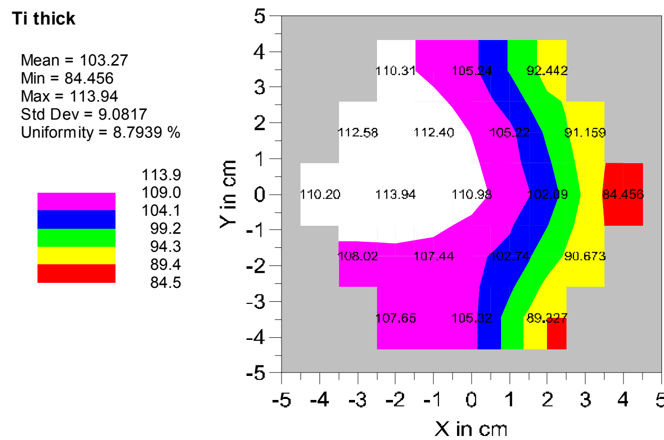

Figure 5.9 – Thickness map of titanium deposition. The titanium is not aligned well.

the center of the chuck needs to be moved 2 cm to the left and 2 cm back. The uniformity of this run was not optimal (8.7%) but centering should improve it. Figure 5.10 shows a closer alignment but still ½ cm off so one more adjustment needed to be done to center it.

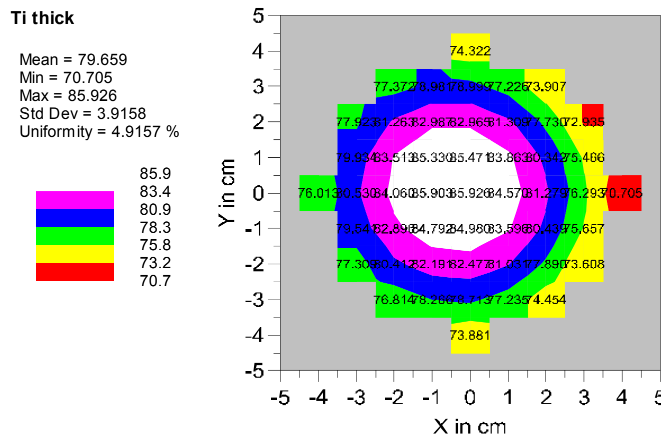

Figure 5.10 – Thickness map of titanium deposition. The alignment is better.

Adding more points in the scan gave a much clearer thickness map. The deposition shown in Figure 5.11 was perfectly centered. It appears the uniformity is still not that good across the wafer (7.5%) but in the center area where the devices are,

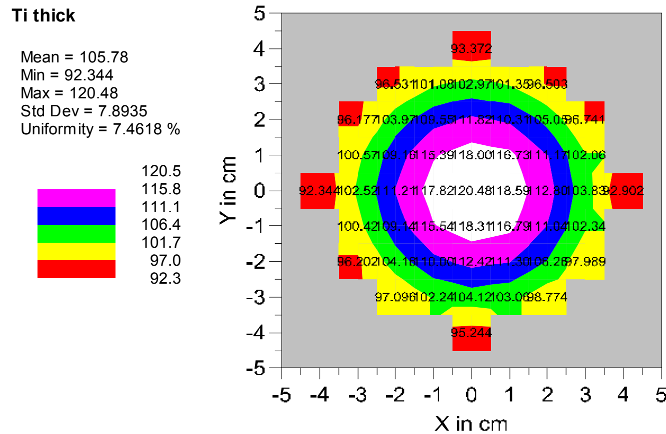

Figure 5.11 – Perfectly aligned titanium deposition.

it is very good. Figure 5.12 shows three titanium depositions run with the target rotated in 90° increments. It seems that the wear on the target can affect the X axis alignment by ½ cm in either direction. When the wafer is rotating (normal usage) this is not noticed. Installing the target in one orientation is discouraged as it makes the wear more uneven

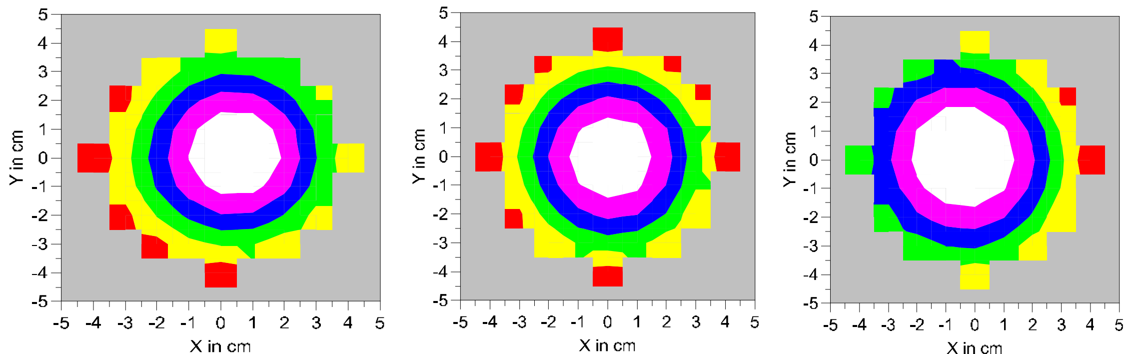

Figure 5.12 – Three titanium depositions showing the effect of target rotation.

Now that the alignment is known, a template had to be developed to align the chuck for each deposition. Since it is not permitted to make marks on the platen, a paper one was

made from cleanroom paper and printed with an inkjet to minimize contamination. Figure 5.13 shows the process of placing the template, lining up the chuck and removing the template. To line up the X axis, the platen is rotated to be under the platinum target

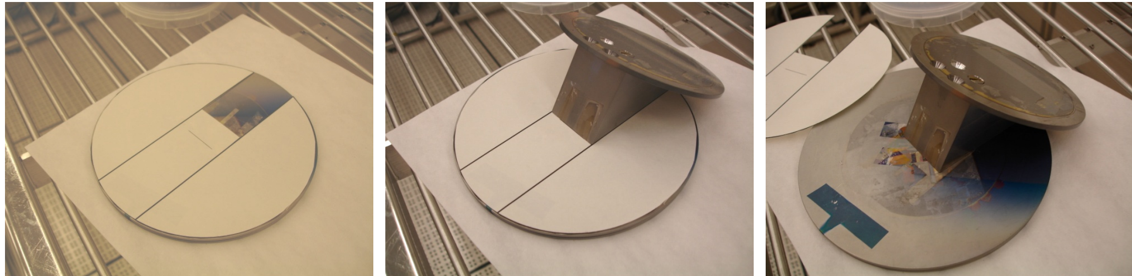

Figure 5.13 – Alignment of the chuck to the platen.

as shown in Figure 5.14 and when the special cleanroom pen held against the gun fits perfectly in the gap between the platen and the wafer, alignment is achieved. At this point, an aluminum foil arrow is taped to the platen which is lined up with the arrow on

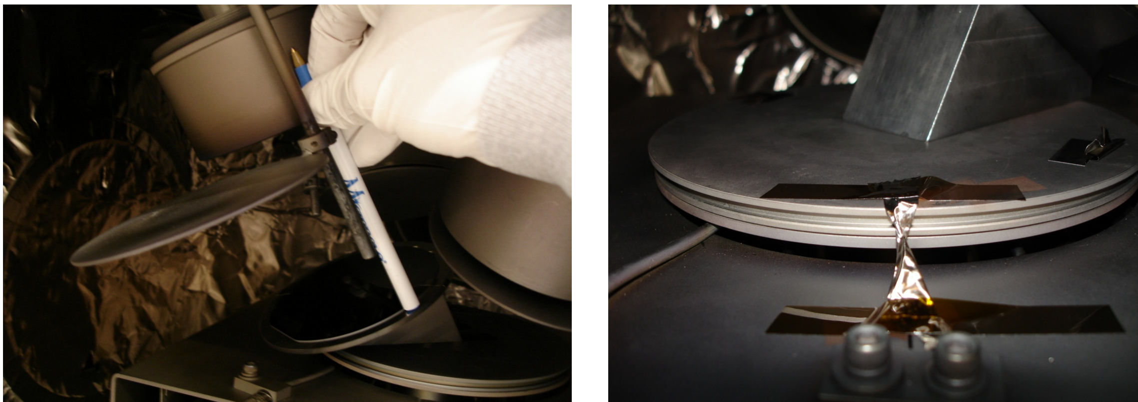

Figure 5.14 – Final alignment of the platen.

the base. Now the platen is rotated and the titanium is lined up. The deposition is now started and when the titanium is done, the motor is used to rotate the platen to align the arrows and the apparatus is ready for the platinum deposition. While this seems like a complicated and time consuming setup, it only takes a few minutes with practice

Shape of the Heater Lines

Once the lift-off process was completed, it was time to characterize the heaters to see if the lift-off was indeed working. My research group at NIST has an AFM that was ideal to look at the heater lines with. Figure 5.15 shows an AFM scan of a line patterned earlier in this project where the lift-off did not work (The SEM image shown in Figure 4.2). There was metal all along the sides but it was so thin and brittle that a

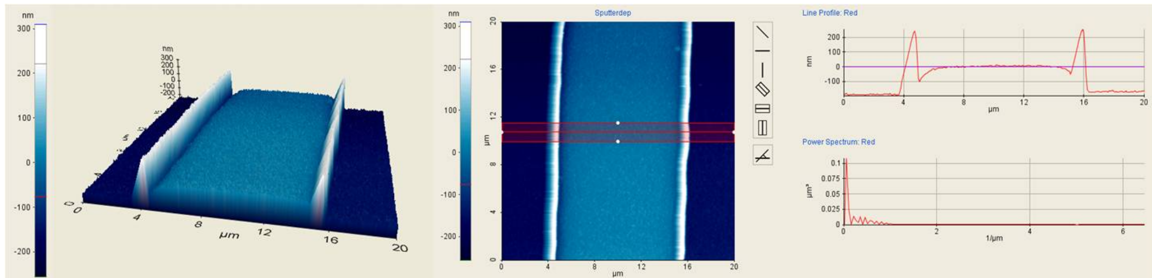

Figure 5.15 – AFM image of line made by lift-off with no undercut.

profilometer just pushed it out of the way and it did not show up on the scan. Figure 5.16 shows an AFM image of a 2 µm line where the lift-off worked perfectly. It is important to note that all of the AFM images have a large multiplier on the Z dimension. So while the trace below in the left looks like a half cylinder, when the z multiplier is changed from 9 to 1 as on the right hand image, it looks much flatter.

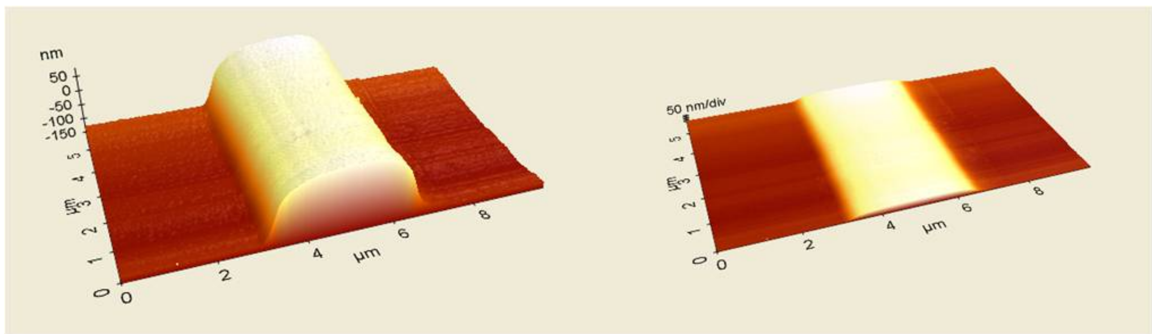

Figure 5.16 – Effect of the Z-multiplier on the perception of the heater shape.

AFM scans were performed on all of the line widths and are shown in Figure 5.17. The 2 μm line was the only one that lost height. All of the lines are their stated width between 80% and 90% of their height except for the 10 μm line which is at 75%. This is shown in Figure 5.18

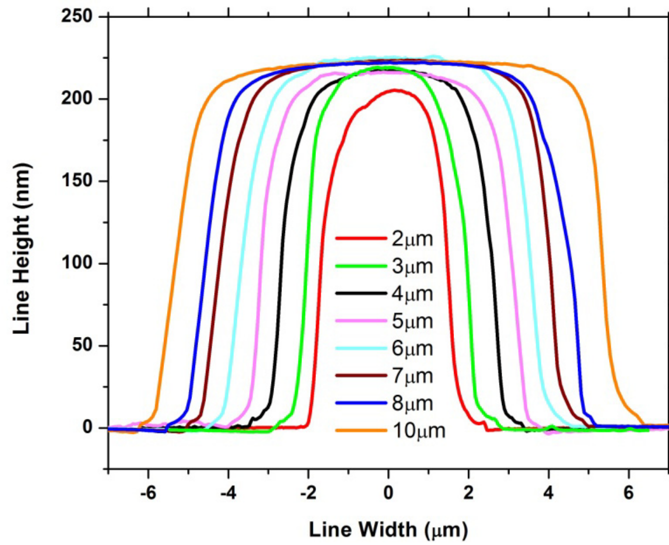

Figure 5.17 – AFM profiles of the heater lines.

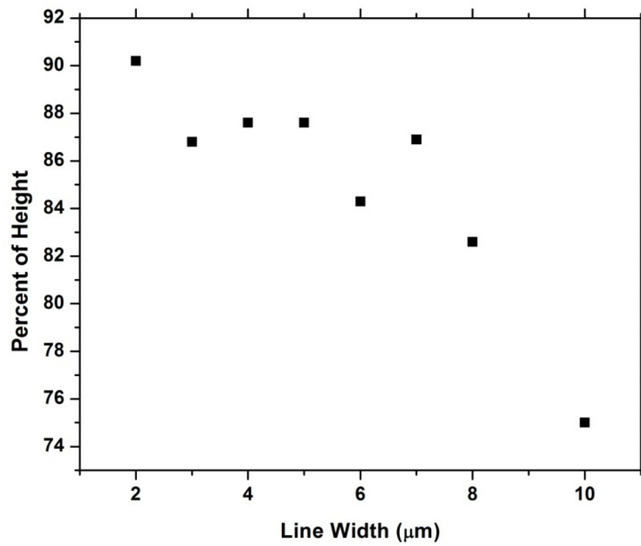

Figure 5.18 – Percentage of height for each lines listed width.

Chapter 6: Stress Management in Films

One of the issues I was concerned about in fabricating metal heaters on thin film membranes is stress. For non-suspended devices this is not a problem however for suspended devices this is an important issue. The end of etching is a critical time for the membrane as it is suddenly released from the substrate. If there is too much stress, the shock of release could shatter the membrane. The stress on the SiN is around 200 MPa tensile which is needed to keep the film from wrinkling. My goal was to create a low stress platinum deposition recipe which would add zero stress to the membrane at 90 °C which is the temperature of the KOH bath when the membrane is released.

Metal Stress Measurement

A FLX-2320 thin film stress measurement system was used to measure the stress on films. This instrument uses a laser scanning system to measure the curvature of a wafer before and after deposition of a thin film. The wafer type and thickness and film thickness is then input and the stress of the film is calculated. One very useful feature of this particular tool is an integrated wafer heater which gives the ability to measure stress at temperatures up to 500 °C.

Initial Stress measurements

For sputter deposited films, the stress on a film is directly related to the chamber pressure during the deposition. Usually lower pressures are compressive and move towards tensile as the pressure is increased. The first material I measured was titanium which is used as the adhesion layer. The stress analyzer showed that the stress was 5300 MPa for a 100 Å thick film. It turns out that the stress chart in the CNST NanoFab was developed only for 1000 Å films and very thin films can have significantly higher

stress. [22]. Since I did not want my adhesion layer to be that highly stressed if it was not necessary, the stress had to be adjusted in the titanium as well. A series of depositions at different pressures shown in Figure 6.1 gave a stress map for the 100 Å titanium films.

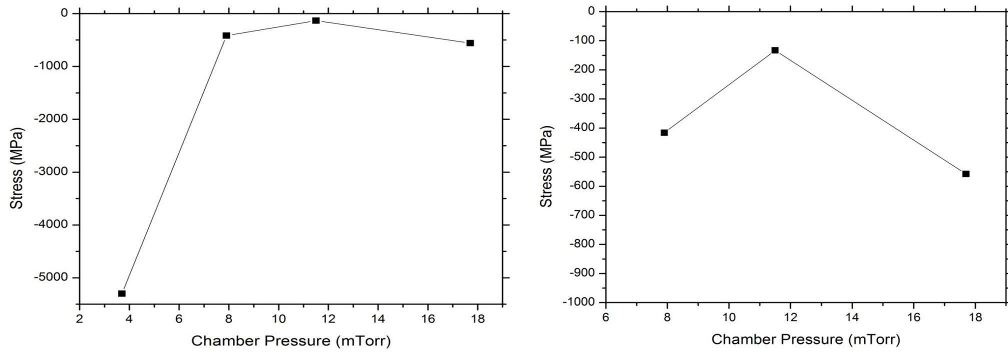

Figure 6.1 – Stress of a 100 Å titanium thin film vs. pressure.

It appeared that the minimum stress is at a chamber pressure of 11.5 mTorr which was obtained with a gas flow of 95 sccm of argon and is well above the listed parameter of 50 sccm. The results for the platinum stress are shown in Figure 6.2. It appears that around 10 mTorr is the lowest stress area.

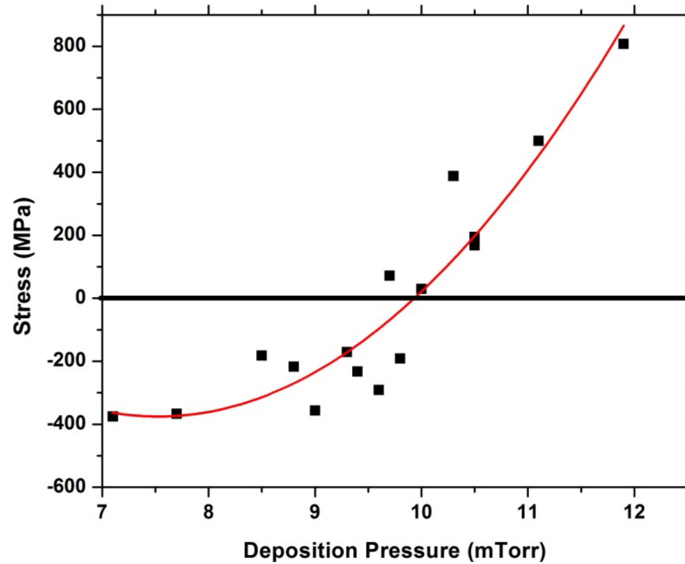

Figure 6.2 – Stress of a 2000 Å platinum thin film vs. pressure.

Stress vs. Temperature in Platinum

The first test was on a wafer with 200 MPa of tensile stress and is shown if Figure 6.3. The temperature was ramped at 5 °C/min to 500 °C (red). The temperature was held for 20 min at 500 °C for the anneal (Green) then the temperature was ramped down (blue). The cooling step took 3 hours to complete. The cooling path is now linear for the

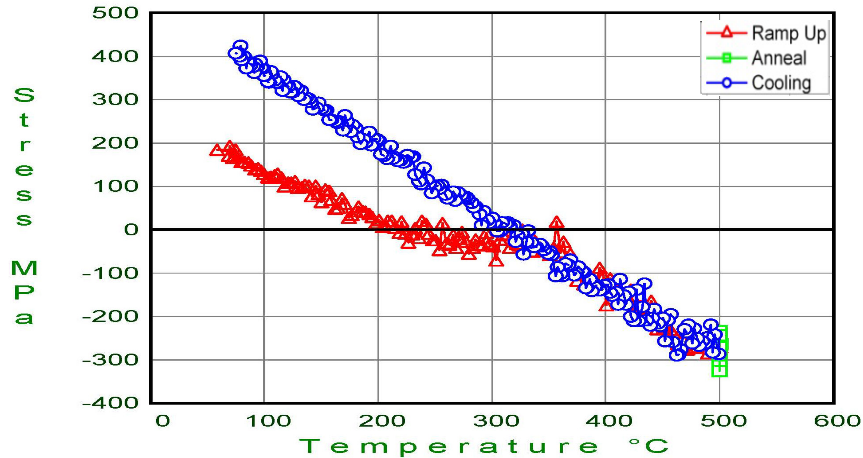

Figure 6.3 – Annealing curve for 200 MPa film.

annealed film. The heating and cooling run was performed again and the results are shown in Figure 6.4 and reveals that the initial anneal time was not sufficient as subsequent runs showed that one hour at 500 °C is required.

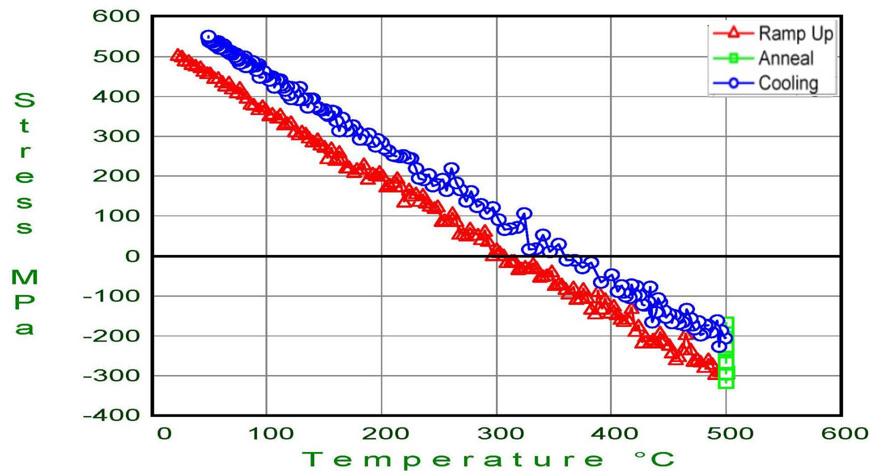

Figure 6.4 – Second anneal showing initial anneal time was insufficient.

Figure 6.5 shows anneal plots for a range of pressures. For my purposes, 6.5(c) meets the criteria of zero stress at the KOH bath temperature of 90 °C and low stress up to 300 °C. This deposition was done at 9.7 mTorr.

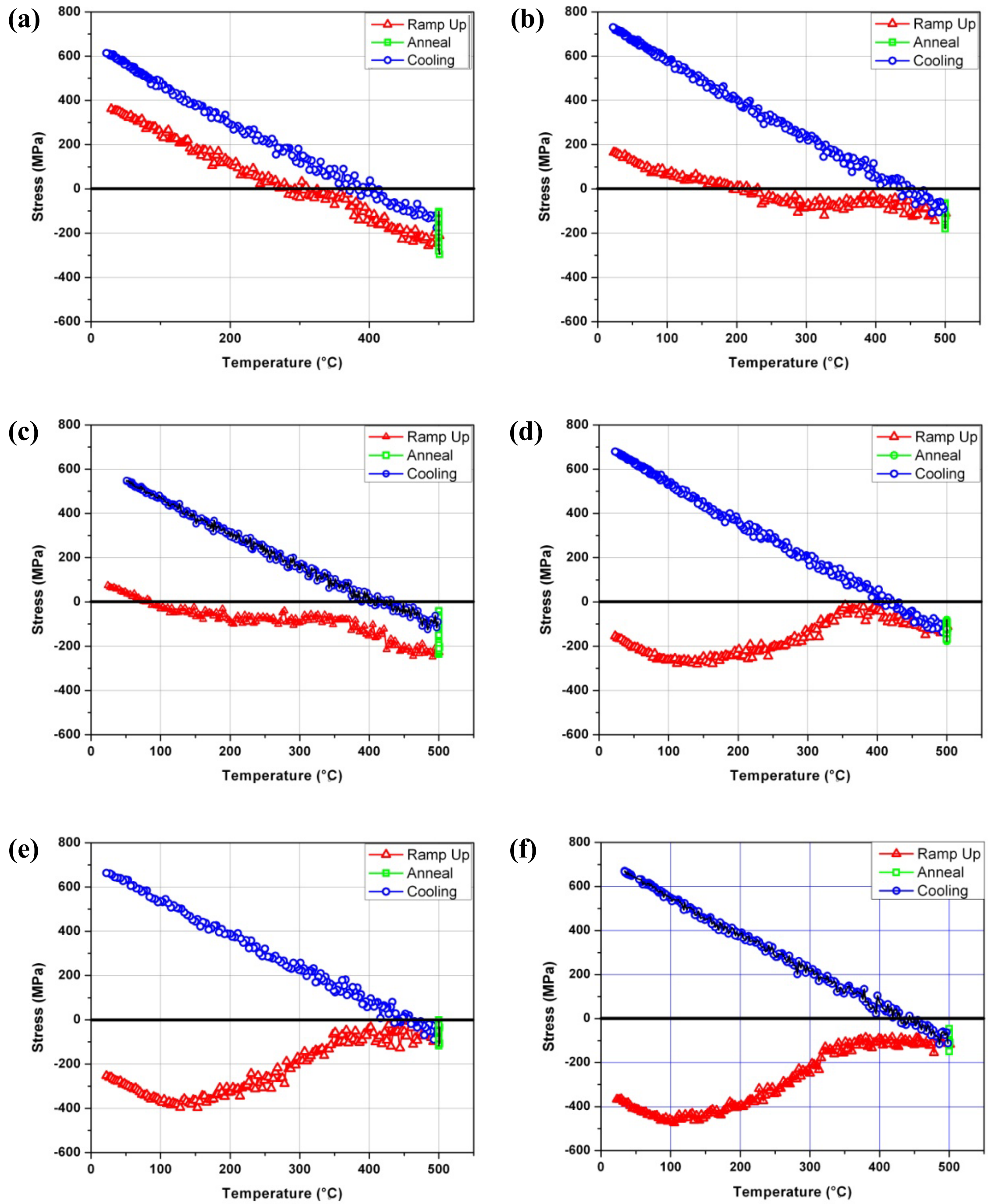

Figure 6.5 – Anneals at various sputter pressures showing the stress differences.

Annealing at 240 °C

Another interesting result is that if the temperature is kept low, there is no permanent change in the film structure when it is heated. Figure 6.6 shows that an anneal at 240 °C has no effect while the one at 500 °C does. This indicates that if the device is operated below 500 °C as it is in the microboiling experiments, the initial stress curve will not change.

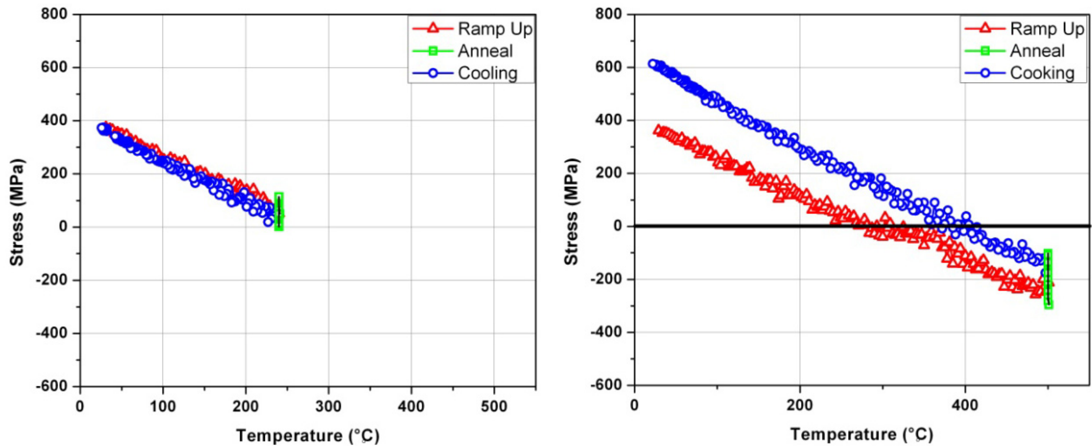

Figure 6.6 – An anneal to 240 °C did not change the film in the same way the 500 °C anneal did.

A Final Test

One of the first fabrications did not go well. Not only was the metal misaligned but the membranes broke as well. Figure 6.7 shows the one of the serpentine heaters with

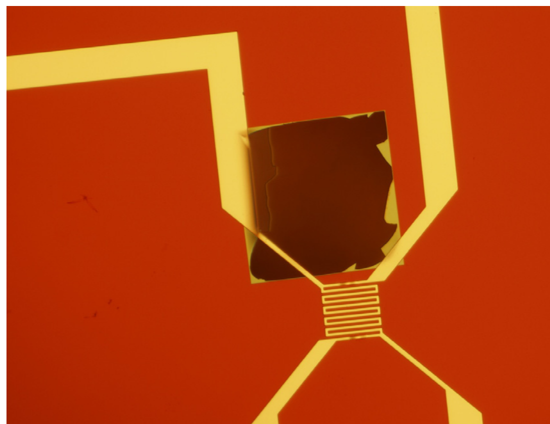

Figure 6.7 – Metal misalignment and membrane destruction.

a sensing line still crossing the gap. While this did not look like a useful device, it still had a use as a 100 µm long, 7 µm wide, 2000 Å thick suspended platinum ribbon. When a current was run through the line as shown in Figure 6.8, the center of the suspended

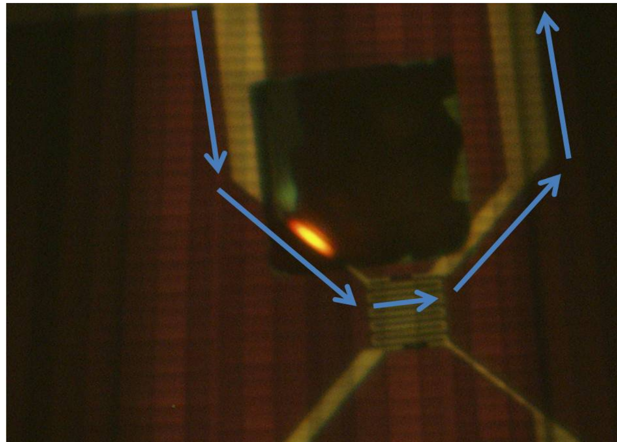

Figure 6.8 – Glowing ribbon heater. The blue arrows indicate the current path.

section glowed quite brightly. The blue arrows represent the current path. When the current was increased to the point where the heater failed there was an interesting result. Figure 6.9 shows that although the lines are separated, they appeared to be a straight cantilevers with very little bending. This indicates that most of the line at least remained at low stress. The heating only lasted two minutes so the remaining metal may not have had time to anneal and increase the stress.

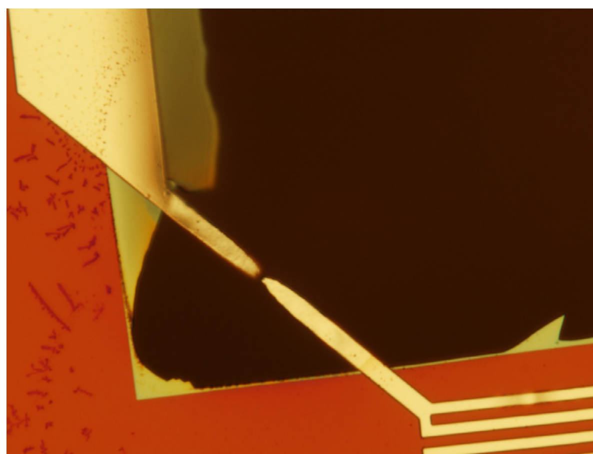

Figure 6.9 – The structure after heater failure. The remaining ribbon is still straight.

Chapter 7: Fabrication

Once all of the processes were optimized, fabrication could occur. This section coarsely describes the process steps involved in getting a single wafer of backside etched devices and then a few initial tests on the devices.

Process Steps

- Wafer Cleaning – RCA clean was done to remove contaminants.
- 2000 Å of low stress SiN grown on both sides in an LPCVD furnace.
- Front side of wafer is coated in photoresist to protect it from the mask steps.
- Membrane mask is patterned on back of wafer in photoresist.
- Mask openings are etched in RIE tool.
- Photoresist removed from front and wafer cleaned.
- Lift-off resist spun on.
- Imaging photoresist spun on.
- Openings for the metal deposition are patterned on front of the wafer.
- Descum RIE process run to clean the surface where the metal will be deposited.
- Sputter deposit 100 Å titanium and 2000 Å platinum.
- Place wafer in 1165 photoresist remover at room temperature overnight.
- Clean any excess metal particles from wafer.
- Place wafer in protection fixture.
- Place in 90 °C KOH bath for approximately five hours.
- Place fixture in 60 °C water bath for 10 minutes to avoid thermal shock.
- Place fixture in HCl solution for 10 minutes to clean off wafer.
- Place fixture in clean water for 10 minutes.
- Place fixture in IPA for 10 Minutes.
- CAREFULLY blow off the IPA with very low pressure nitrogen.
- Remove wafer from protection fixture.

Device Inspection

The die were separated with no problems and then inspected. The completed membrane devices are shown in Figures 7.1 and 7.2.

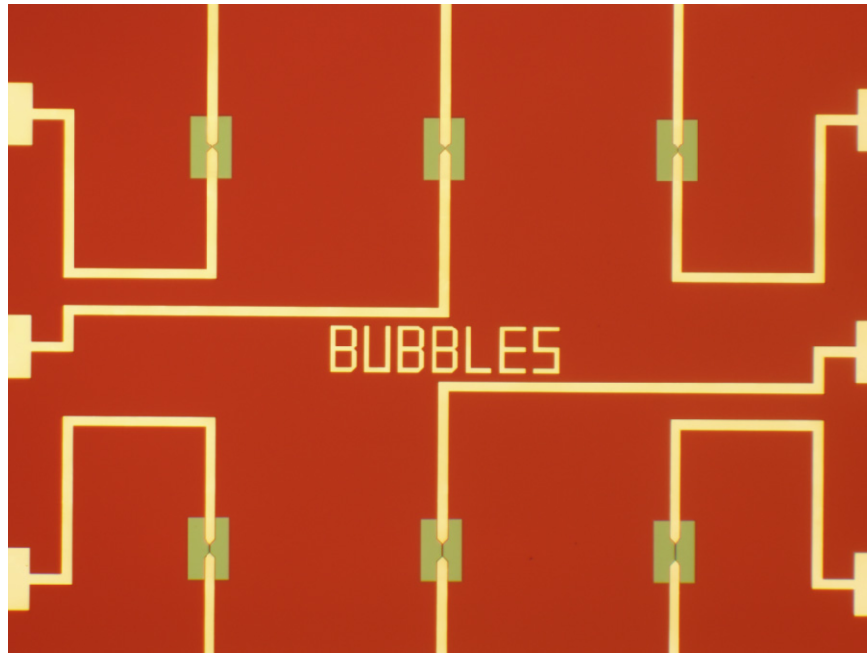

Figure 7.1 – Completed bubble heaters on membranes.

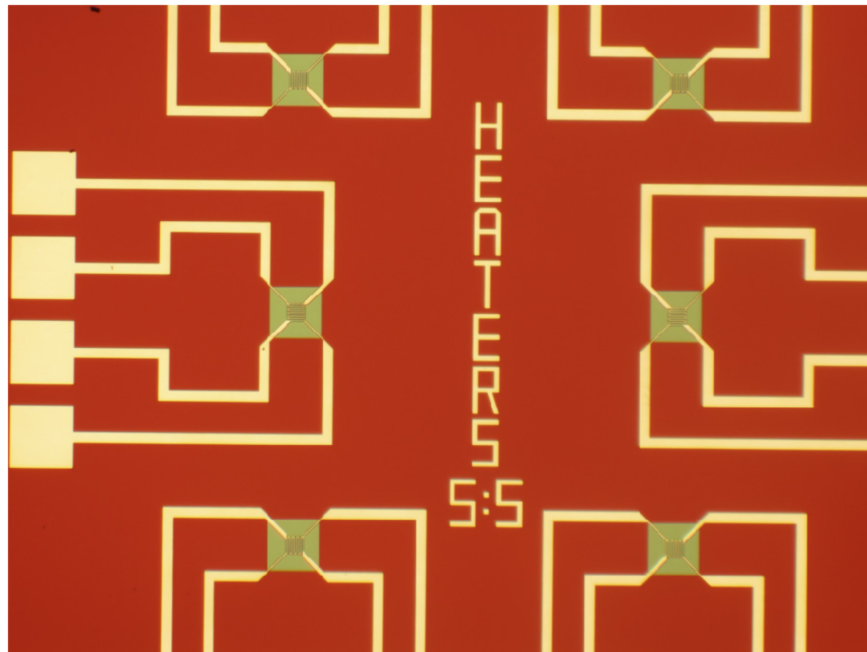

Figure 7.2 – Completed microhotplates on membranes.

The device for the nanoheaters also came out well as shown in Figure 7.3. There was no lift-off residue or stray metal in the separations between the heaters and the shield.

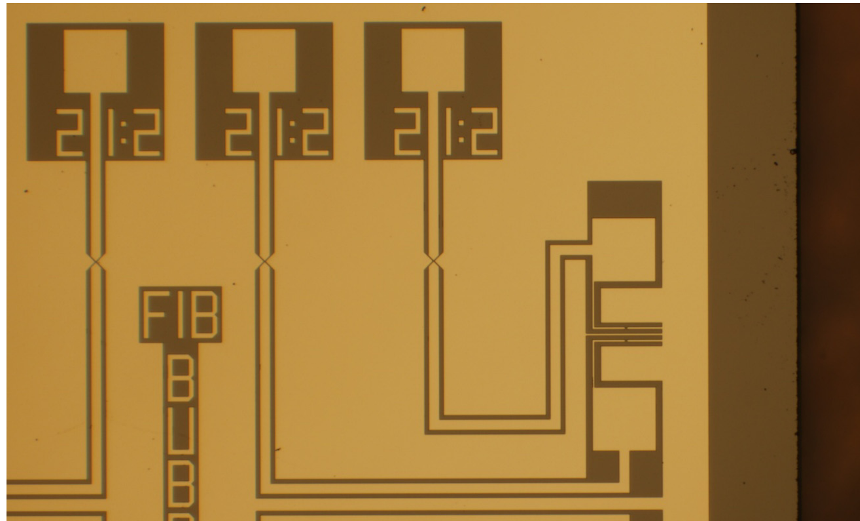

Figure 7.3 – Completed shielded nanoheater device.

Membrane Test

To test the effect that heat had on the membranes, the microhotplate device was connected to power using a probe station and voltage was applied until the heater glowed red as shown in Figure 7.4(a). The temperature was estimated to be 600 °C to 700 °C from the color. After five minutes the power was turned up until it was glowing bright yellow at which time it failed as shown in Figure 7.4(b). The platinum film failed even though the temperature was well below its melting point (1772 °C). Apparently,

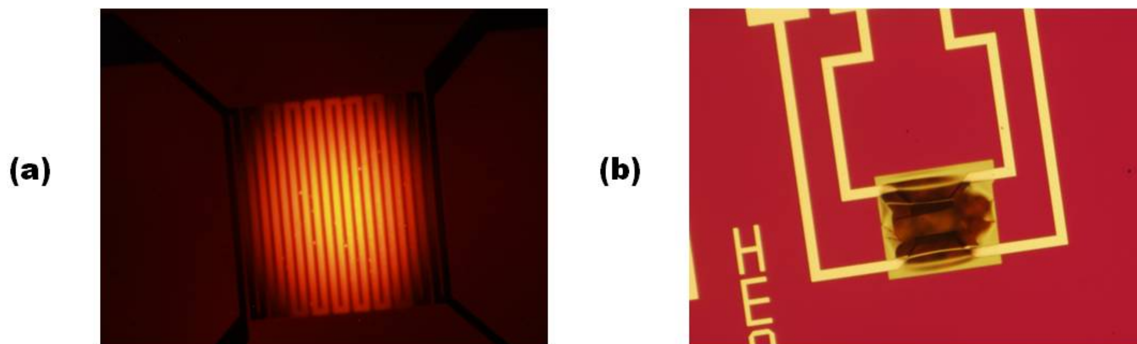

Figure 7.4 – Glowing microhotplate (a) and blown out membrane (b).

platinum thin films will degrade in air and form islands starting at 900 °C [23]. From this simple test, it was shown that the membrane would easily handle the 300 °C to 500 °C microboiling experiments.

Temperature Coefficient of Resistance

To measure the TCR of the device, the microhotplate device was wirebonded to a 40 pin package and was placed in a tube furnace where it was heated up to 248 °C while the resistance was being measured. The slope of the resistance increase was measured and plotted in Figure 7.5.

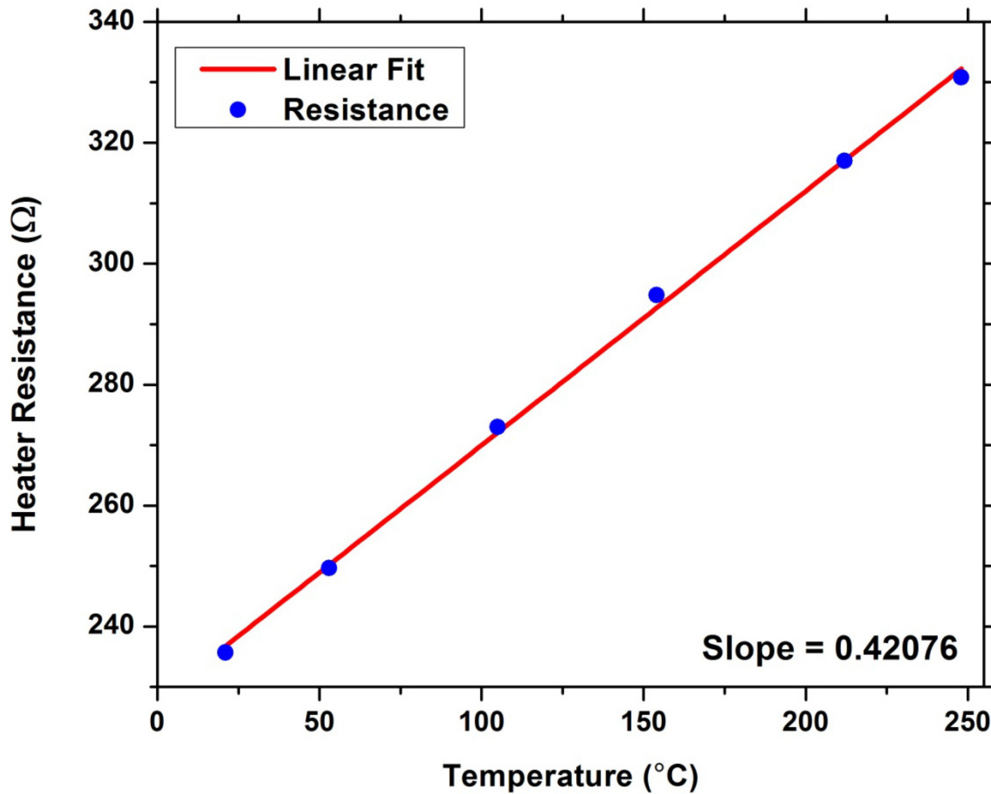

Figure 7.5 – Resistance vs. temperature for platinum heater.

The TCR was calculated by dividing the slope by the room temperature resistance. This gives a value of 0.001785 /°C. The TCR of bulk platinum is 0.0039 /°C so this value for a thin film was expected.

Chapter 8: Packaging

While the design and fabrication of the actual wafer level part of the devices was a major part of the creation of the bubble heaters, packaging was also a critical element. What seems like a trivial part of the project actually required significant innovation to complete due to the unique issues facing devices fabricated on membranes as well as devices immersed in solvents. Because the fixtures I used in the tests included a 40 pin ZIF (Zero Insertion Force) socket, the heater die needed to be mounted into a 40 pin DIP (Dual Inline Package) for easy connection to the electronics.

Dicing

Since these devices are going to be tested in both a suspended and non-suspended configuration, the wafer design needed to be set up to allow for the option for of having the dicing done by either the KOH etch or a dicing saw depending on what type of device was being made. Chapter 3 describes the dicing lines as part of placing the die designs on the wafer.

Dicing - Suspended Devices

The KOH etched devices have scribe lines etched into the backside of the wafer and the die were separated by snapping them apart. This was not the optimal scribe line design as mentioned in the etching chapter but the membranes were strong enough that the slight shock of the snapping did not damage them. The scribe lines were oriented such that the devices broke into horizontal strips which were then separated into individual devices (Figure 8.1).

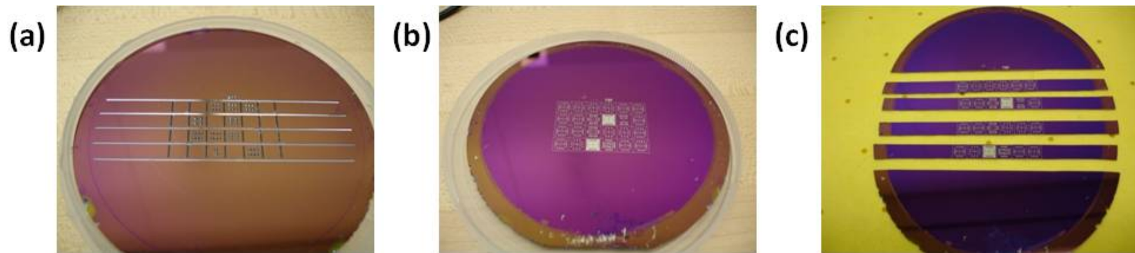

Figure 8.1 – KOH etched wafer showing the scribe lines on the back (a), the devices on the front of the wafer before separation (b) and the separated strips of devices (c).

Dicing – Non-Suspended Devices

For the non-suspended devices, the die were separated with a Disco Model 341 wafer dicer using a metal blade. The dicing was simplified because of the 10 μm metal guide lines between the die on the wafer. Before dicing, the wafers needed to be coated in photoresist to protect them from the slurry created from the silicon particles which were generated as the wafer is being cut.

Die Attachment

The non-suspended and suspended devices now needed to be mounted into the packages prior to wire bonding and testing.

Die Attachment – Non-Suspended Devices

For the non-suspended devices, this was a trivial step. The die were fastened to the center of the 40-pin package with fast drying epoxy and allowed to dry overnight before wire bonding.

Die Attachment – Suspended Devices

For packaging the suspended devices, it is important to consider the etch pits on the bottom of the die. For proper operation, the device needs to be completely sealed to

the package to prevent fluid from getting onto the back of the membranes. When the prototype devices were tested on a probe station, the liquids wicked underneath the device and got into the backside etch pits. However, by simply gluing it to the package, there was air in a sealed space which could expand when heated and burst the membrane as well as the possibility of glue filling the pits. The way to circumvent this was to drill a small vent hole into the package and mount the device over it. This created the problem of having a rectangular set of openings and having to precisely align them to a hole in the package as well as not getting epoxy in the pits or the hole when attaching the die. The solution to this problem was to place spacer with a square opening between the device and the package. As a test I used one of the large area membrane samples from the etch tests and removed the membrane to create the spacer. With a spacer, the epoxy could be applied to the surface of the spacer very thinly and then the device is attached to it without getting epoxy in the pits. When the assembly is dry, the epoxy is applied to the bottom of the spacer and it is attached to the package. The use of a spacer makes the size, shape and precise location of the hole not critical as long as it fits in the spacer opening which is 4 mm. Figure 8.2 shows a schematic of the process.

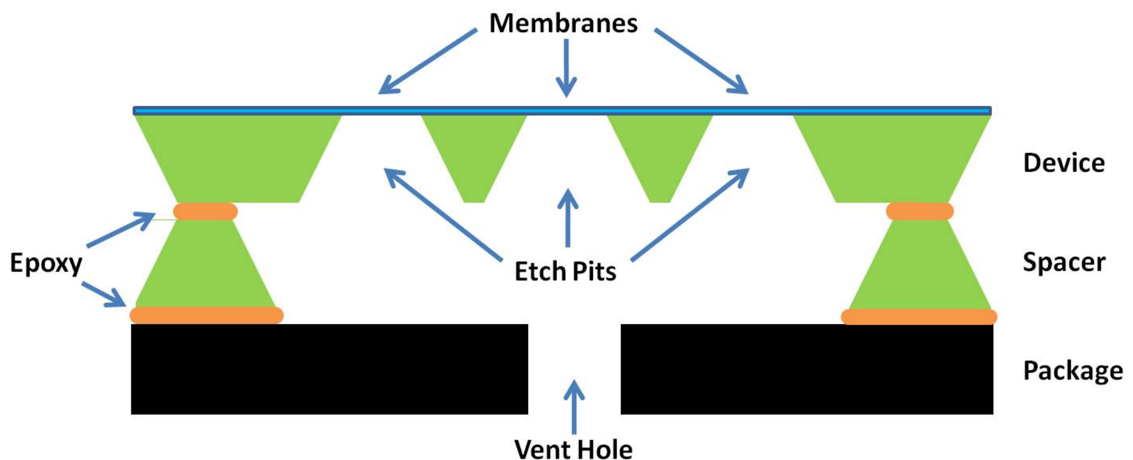

Figure 8.2 – Schematic of the device mounting showing the device, spacer and package.

Figure 8.3(a) shows the backside of the etched device including two of the six etch pits. Because all of the edges of the KOH etched devices are sloped, it is difficult to see the edge of the front of the device so it is highlighted with a red line in the figure. Figure 8.3(b) shows the backside of the spacer after the membrane was removed. As in the previous image, the red line highlights the edges of the spacer. Figure 8.3(c) shows a spacer aligned with the back of the device. The dotted lined show where it will be attached with the epoxy on the back of the device. This spacer was from the initial etch

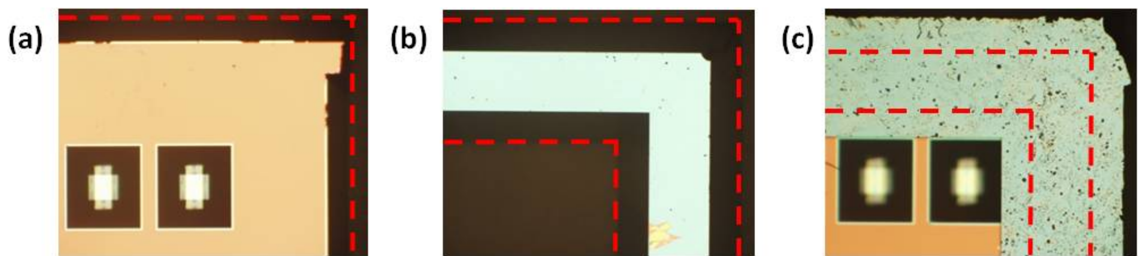

Figure 8.3 – (a) The backside of the device showing the etch pits. The red line shows the edge of the front of the device, (b) The backside of the spacer. The red line shows the edges of the front of the spacer. (c) The spacer aligned with the device. The red line shows the attachment point.

tests and was not protected from dust as it would have been if it had been known that it was going to be needed A new mask was fabricated to create a wafer of spacers but the first test of the spacer mask did not work well. The scribe lines which were used did not go all the way through the wafer. The spacer arms were too fragile and snapped apart when attempts were made to separate them. A redesign was done using the original scribe lines that went completely through the wafer. Because the frontside protection fixture was not used, it could be seen exactly when etching was completed. Also etching went faster as the ultrasonic agitation could be kept on throughout the entire etch because he membranes needed to be removed at the end of the etch. As the packages are made from ceramic, the options for making a hole are limited. A regular drill bit will not cut ceramic

and an attempt to use a diamond tip drill caused the package to shatter. This left the option of laser drilling or an ultrasonic drill. The shop facility at NIST had an ultrasonic drill and ran a test which worked great. They drilled an approximately 1 mm hole in center of the package with no chipping at the edges as shown in Figure 8.4.

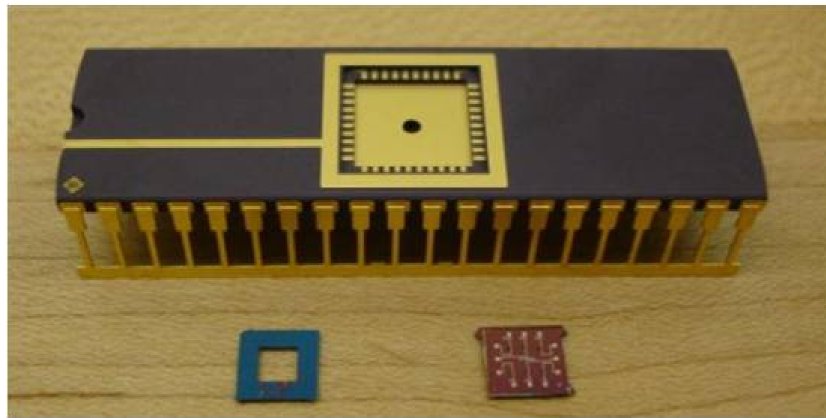

Figure 8.4 – 40 pin DIP package with 1 mm vent hole drilled in it, the spacer and the finished device ready to be assembled.

Wire Bonding

Attaching the bond pads of the devices to the pins on the DIP was actually the least problematic part of the packaging. A Kulicke & Soffa wedge wire bonder was used to attach 1 mil gold wire from the bond pads of the devices to the package pads as shown in Figure 8.5.

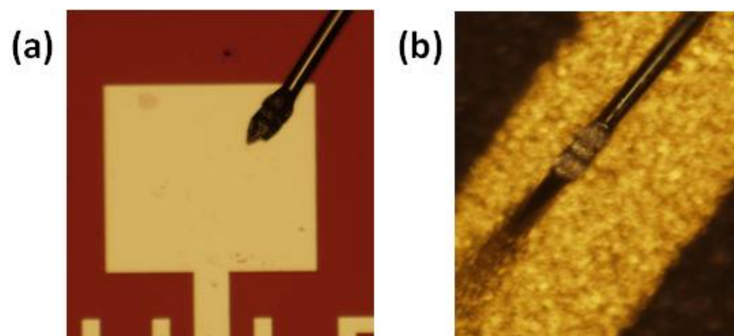

Figure 8.5 – (a) Gold wire bonded to the device bond pad and (b) the DIP package pad.

After the first test of the wire bonding, the bond strength was tested by attempting to pull the wire off of the bond pad which snapped the wire before the bond failed. This test also shows that the metal adhesion is very good as bad adhesion can result in the bond pad being ripped off of the substrate.

Fluid Reservoirs

The final packaging issue that occurred is what to do if solvents are being used as the test liquid. Water will bead up due to surface tension and form a nice thick droplet on the device that will remain for an hour or more (Figure 8.6(a)). Methanol however, wets the device and package and evaporated during a test (Figure 8.6(b)). Another problem

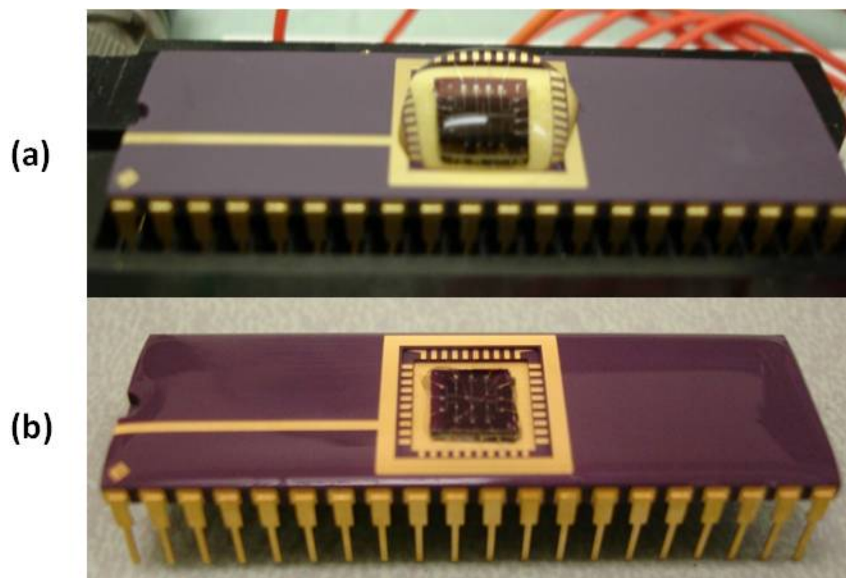

Figure 8.6 – Water beading on the device (a) and methanol conformally coating the surface of the package (b). It is not shown but the bottom surface is coated as well.

is that the solvent not only wets the top but flows onto the bottom surface and then wicks up into the vent hole resulting in solvent on the back of the membrane. To avoid this, a reservoir needed to be created to hold the liquid. As it turns out, there were some square plastic cuvettes which were the exact size as the outer potion of the package opening. Cutting off a segment and filing the edges smooth gave a square piece which was open on

each side that attached to the package with epoxy to create a reservoir (Figure 8.7). Their resistance to solvents was tested by filling one with methanol and another with ethanol

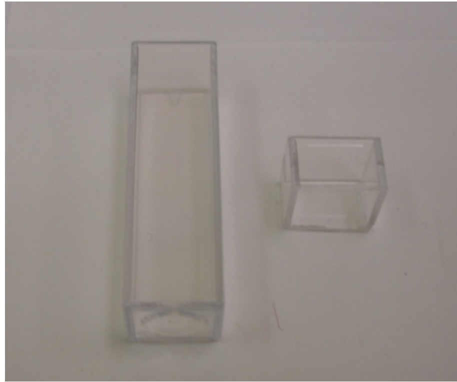

Figure 8.7 – Uncut and cut plastic cuvettes.

overnight to see if the solvents attacked the plastic and there was no visible problem seen. The completed device is shown in Figure 8.8. In the tests on solvents, there was enough liquid in the reservoir that the evaporation was never a problem during the experiments.

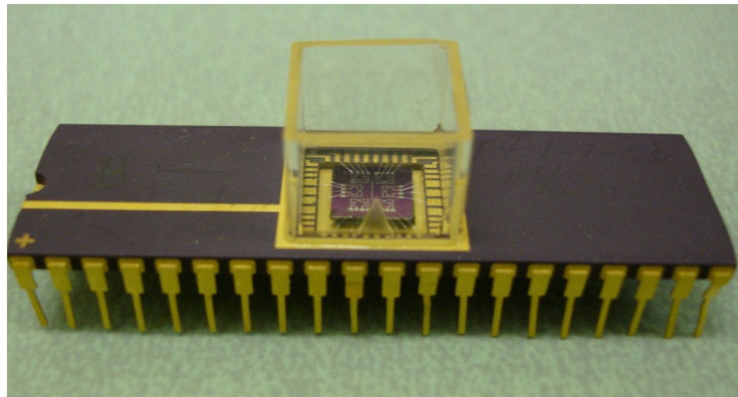

Figure 8.8 – The packaged device ready for testing.

Chapter 9: Testing

The tests on the devices consisted of capturing the signal formed by a bubble nucleating in water using the suspended and non-suspended devices of varying widths and W/L ratios. Ethanol was tested next to investigate the increased sensitivity of the new devices.

Experimental Setup

A Wheatstone bridge along with a differential probe was used to characterize the nucleation event on a digital oscilloscope. The setup is shown in Figure 9.1. The

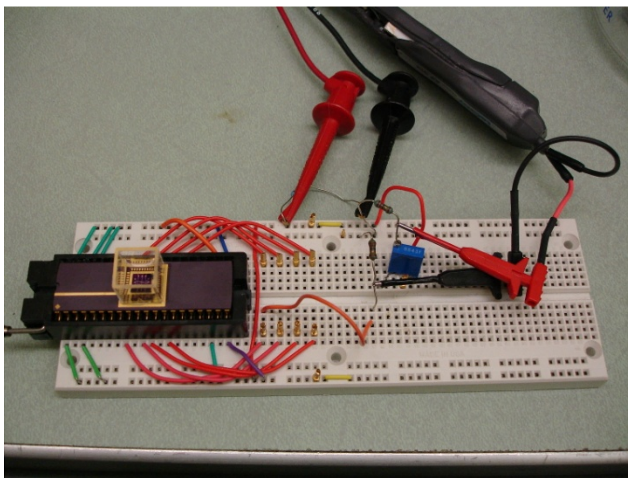

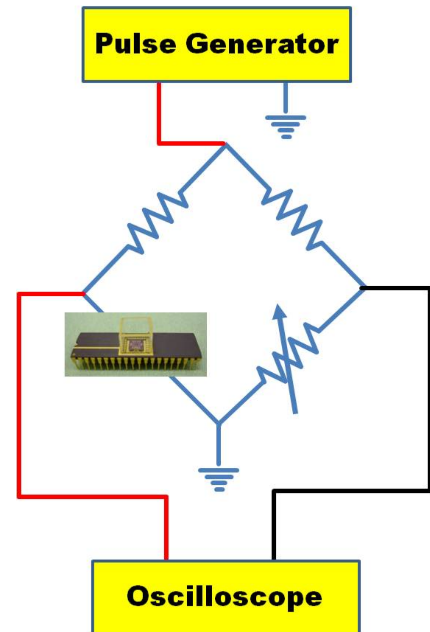

Figure 9.1 – Data acquisition circuit.

breadboard test structure was designed to allow rapid testing of multiple heaters in a package. All of the grounds were preconnected and there are signal taps to allow the measurement of the resistance. The procedure was quite simple, once the device was connected, a single wire was connected to the input pin and the power supply was set to 2.00 V. The heating pulse width was set to 5 μS at a frequency of 30 Hz. The variable

resistor was adjusted to balance the bridge at which point the voltage was increased until the inflection point was observed. For consistency, the voltage was adjusted such that the inflection point occurred at 4 μS. While this was a very convenient system to use, it did introduce a lot of noise in the first 1 μS. For pulse widths much shorter than the 5 μS which were used in these tests, a multi layer printed circuit board with ground planes and integrated filters will need to be designed and used. Figure 9.2 shows the complete experimental setup used to acquire the data.

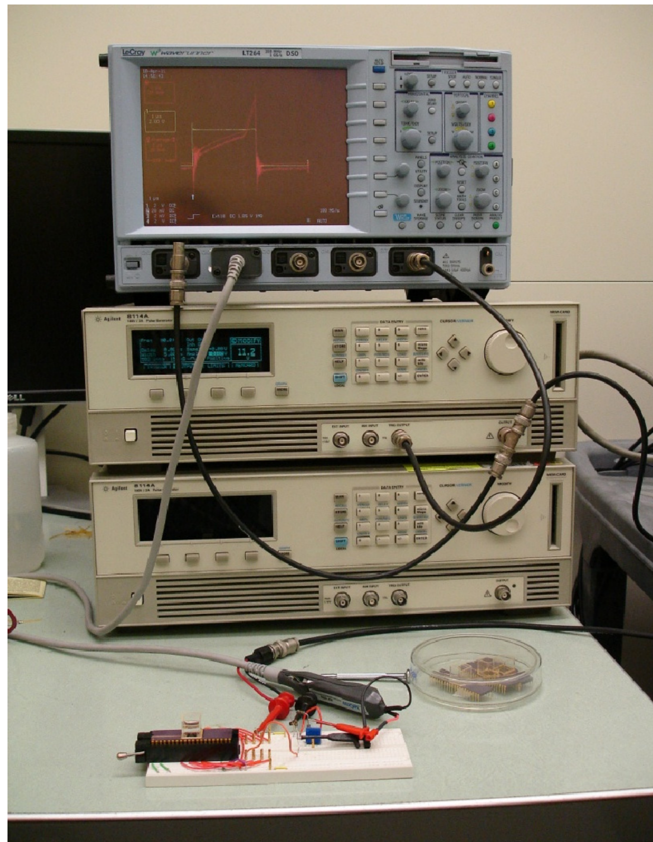

Figure 9.2 – Bubble nucleation experiment setup.

Figures 9.3-5 shows the results of the heater tests in water for the 6 μm, 4, μm and 2 μm suspended and non-suspended devices. Figure 9.6 shows the results of the 2 μm suspended and non-suspended devices in ethanol.

6 μm Heaters - Water

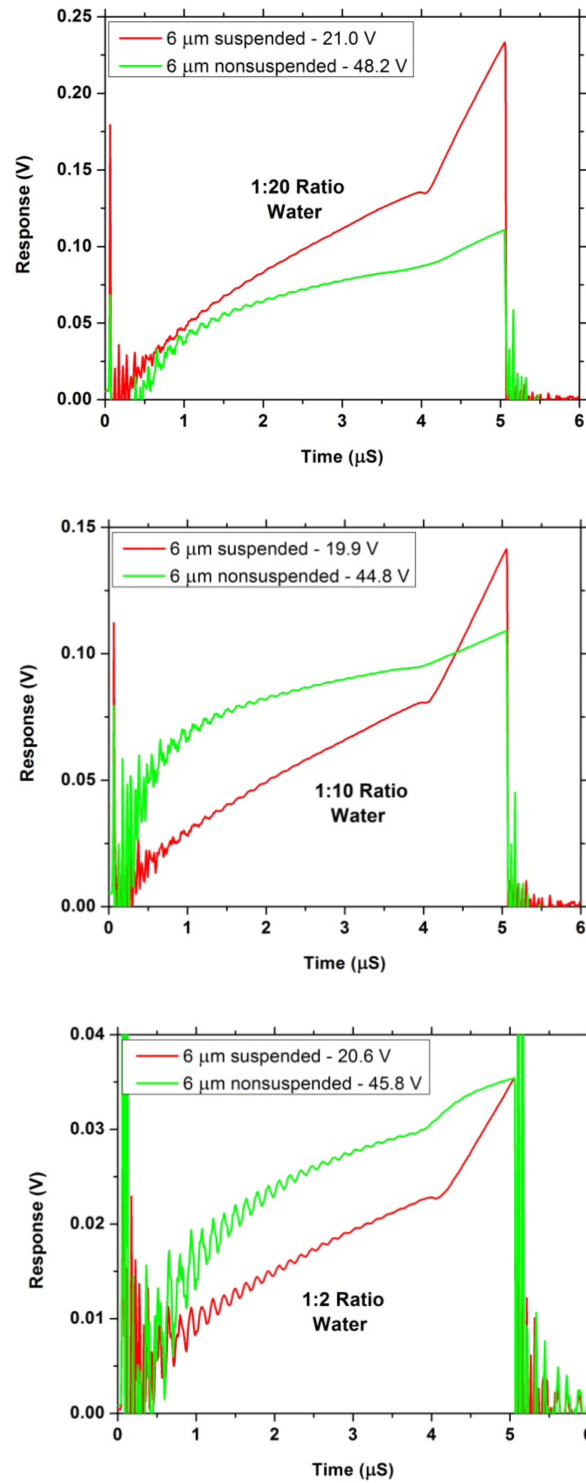

Figure 9.3 – Bubble nucleation in water for 6 μm heaters.

4 μm Heaters - Water

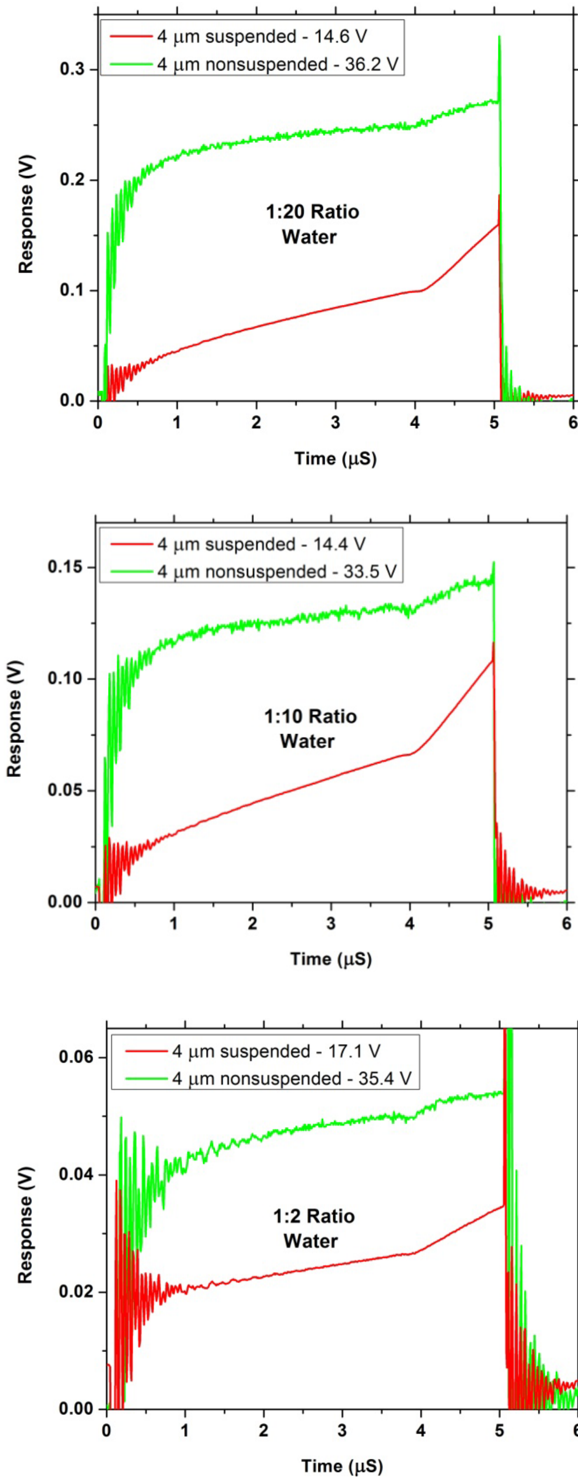

Figure 9.4 – Bubble nucleation in water for 4 μm heaters.

2 μm Heaters - Water

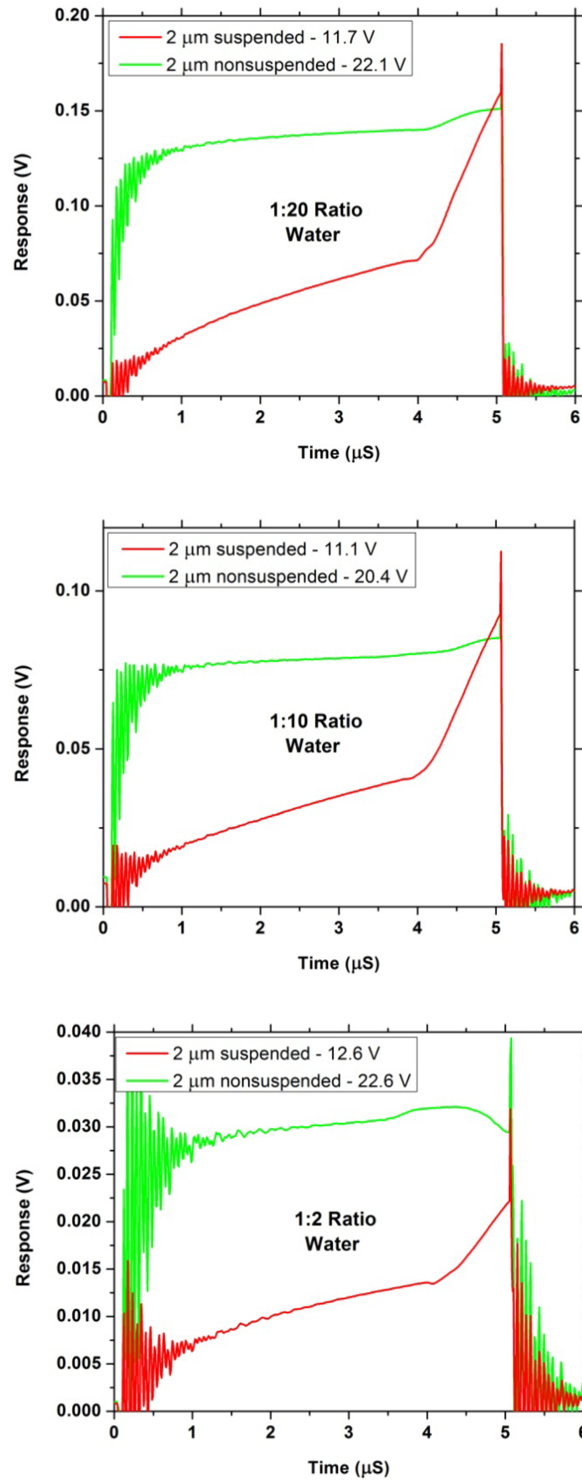

Figure 9.5 – Bubble nucleation in water for 2 μm heaters.

2 μm Heaters - Ethanol

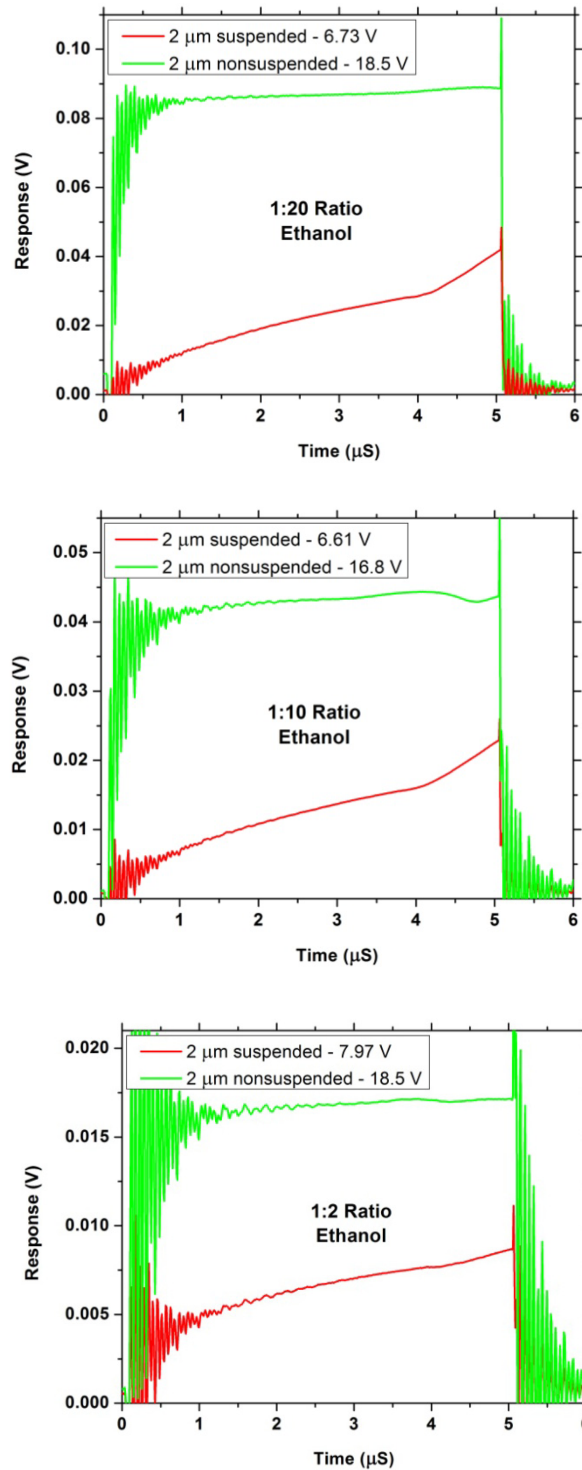

Figure 9.6 – Bubble nucleation in ethanol for 2 μm heaters.

Discussion of Results

All of the suspended heaters which were tested, whether in water or ethanol, showed a dramatic increase in the ability to detect the inflection point and the slope. It is especially noticeable as the heater width goes down. In all cases the applied voltage to reach the inflection point was cut at least in half for the suspended devices. One thing that is noticeable in these results is that the amount of noise in the early part of the pulse increases significantly as the W/L ratio drops. It was also seen that the input power decreased as the heater width decreased which was consistent with the results of Deng, Lee and Cheng [10]. It appears that the W/L ratio has an effect on the sensitivity as well as the width of the heaters decreases. In Figure 9.5, the 1:20 device shows a much larger change in slope than either the 1:2 or 1:10 devices. This may have to do with the heat being more uniform in the center of the ribbon away from the thicker metal of the leads. In Figure 6.9, the heater burned out exactly in the center of the ribbon where it was the hottest. It will be interesting to see if the bubble forms in the center of these in the next phase of this research when the bubbles are imaged.

Chapter 10: Creation of Nanoscale Heaters

Fabrication of nanoscale heaters (250 nm) requires procedures beyond conventional lithography.

There are two methods which could be used to create these nanoheaters.

1. E-Beam lithography.
2. Standard optical lithography to make the smallest heaters possible combined with Focused Ion Beam (FIB) milling. There are two ways to make the heaters shown in Figures 10.1 and 10.2. Figure 10.1 uses the FIB to remove all of the metal from around the heater but takes a long time to make. Figure 10.2 is much quicker because it electrically isolates the heater with much smaller cuts. One drawback is that redeposition of metal could occur during milling and short circuit the device.

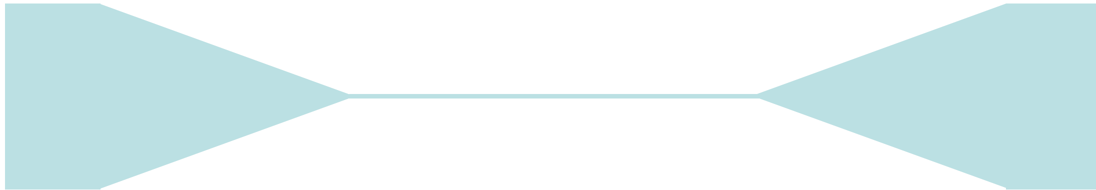

Figure 10.1 – Creation of heater by removing all unwanted metal.

Figure 10.2 – Creation of heater by electrically isolating the metal strip.

From a cost/flexibility standpoint, the FIB approach was chosen as the E-Beam is $375.00/hr vs. $100.00/hr for the FIB. Also, using the FIB allowed for the use of many “starting point” devices fabricated with optical lithography and the heaters could be created one at a time with many different patterns.

A Focused Ion Beam consists of a beam of heavy ions (in this case gallium) which are focused down into a thin beam to mill away the target material. The tool has several modes one of which is coarse milling which can be used to remove large amounts of material but with reduced accuracy. A second mode is fine milling with a narrow low power beam to do final smoothing. The ion beam can be used for imaging, similar to an electron beam, however some milling of the sample occurs. That is why there is also a SEM built into the FIB system. There can be issues with alignment between the FIB and the SEM and that can cause issues with aligning multiple cuts as seen in the figure below. The first attempt used the isolation method to make the heater. Figure 10.3 shows the

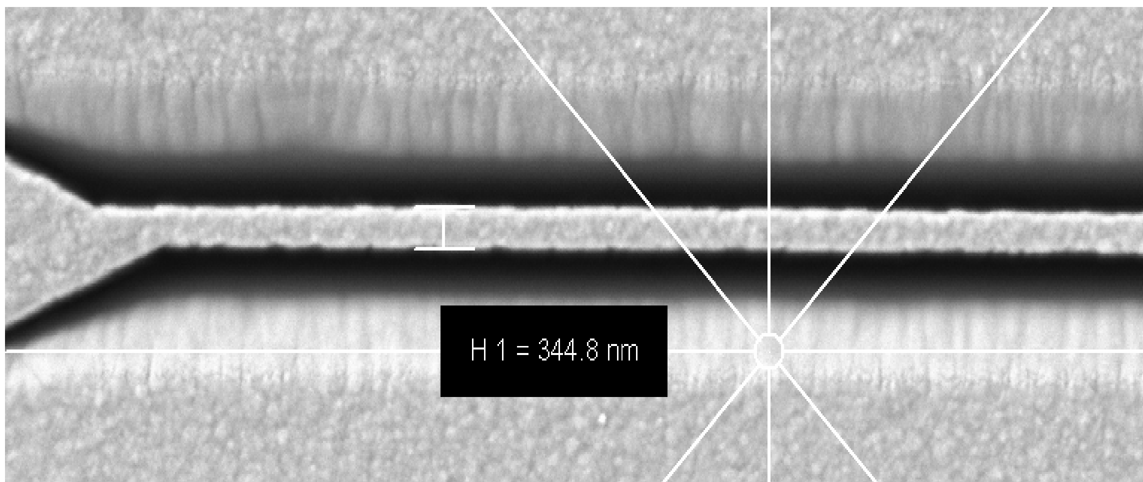

Figure 10.3 – SEM image showing 345 nm heater.

initial cuts of the ion beam. It made a coarse cut through the metal and created a 344 nm wide strip. The initial pass used a mode called "Cross Section" which gives sloped edges around the cut instead of a square trench so that the sample can be tilted to view the depth of the cut. This was useful to adjust the power to minimize excessive etching of the substrate. The next step was to use the fine beam to shave the line down further until it was the desired size.

Unfortunately during the time it took to make this first pass, the SiO_2 substrate became extremely charged (Figure 10.4) and caused an arc to the ion gun and blew an impressive

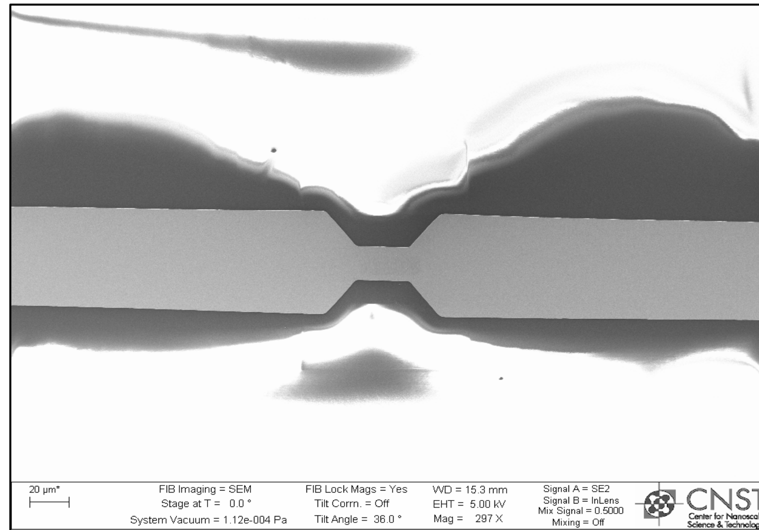

Figure 10.4 – SEM image showing massive charging.

hole in the device (Figure 10.5). This problem was fixed by surrounding the devices with metal which was grounded to the FIB sample holder and absorbed the charge leaving a minimum of exposed dielectric.

…..

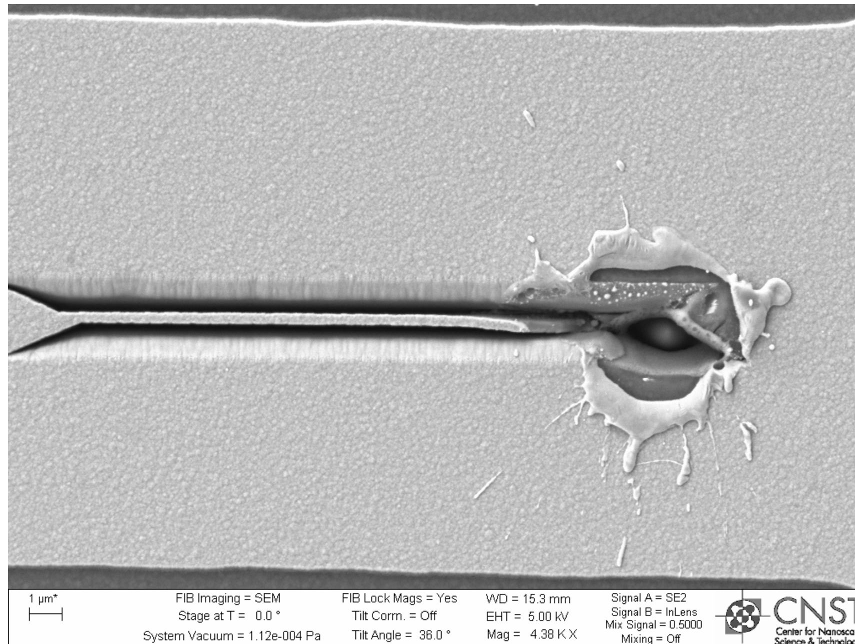

Figure 10.5 – The catastrophic result of a large arc due to charging

Design of Shielded Devices

The first try at shielding was to deposit metal around all of the devices to absorb the charge. The devices were still isolated and that caused some visible charging. Aside from arcing, charging also has the potential to reduce the accuracy of the milling so the design was changed to remove even more of the charge. The new design essentially has all of the devices and the ground shield connected to each other. One bond pad from each device is connected to the ground plane by a thin line with a very thin 2 μm link which can be quickly cut with the FIB to make the devices isolated again. This allowed a single mounting clip on the FIB to ground everything. The links are thin enough (very fast to cut through) and far enough away from each other to keep the device from charging up while cutting them. Also, the maximum power on the FIB could be used since accuracy is not critical and only need a one pass cut. Figure 10.6 shows the CAD design of the die drawn in LEdit.

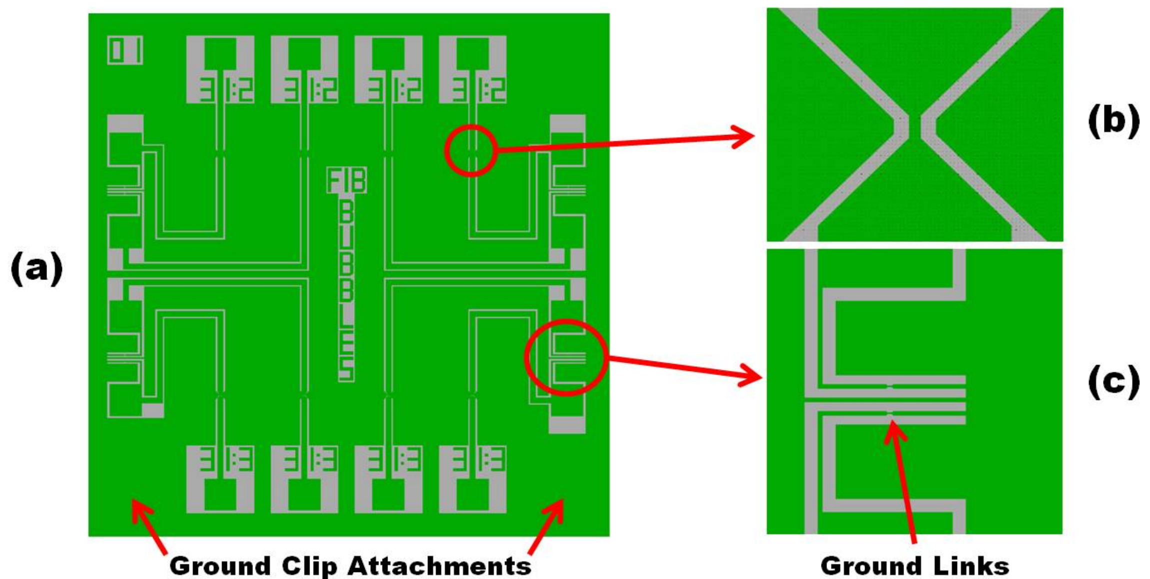

Figure 10.6 – LEdit drawing of the device showing the heater and ground links.

The fabrication of these devices was successful as shown in Figure 10.7 which shows the ground plane, surrounded heater and the ground links. The device was then placed in the

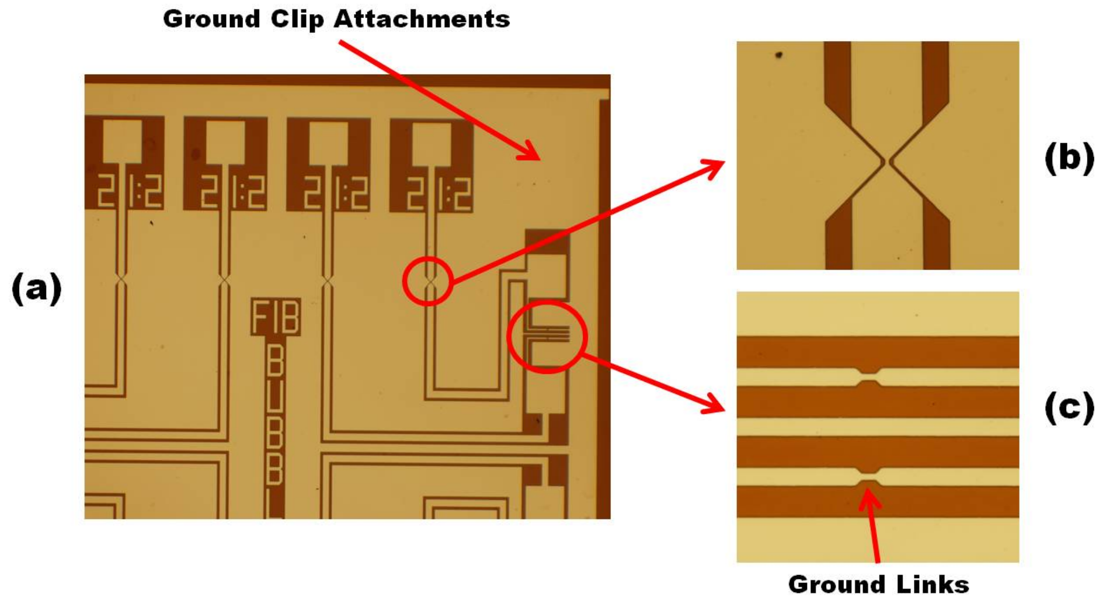

Figure 10.7 – The actual fabricated device showing the heater and ground links.

FIB and the ground clip was attached. It was imaged in SEM mode for a few minutes and there was absolutely no visible charging as shown in Figure 10.8.

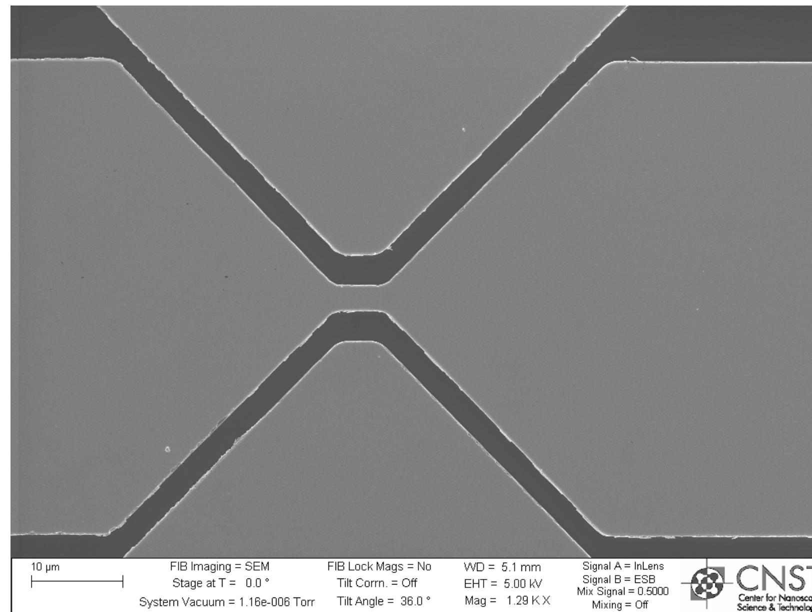

Figure 10.8 – SEM image of the 2 μm heater surrounded by and grounded to the metal shield. There was no visible charging at all.

Milling the Devices

The first pass of the ion beam cut partway through the metal (Figure 10.9) and the cutting with the coarse beam took four passes. Due to some alignment errors in the tool, the top and bottom trapezoids are not perfectly aligned but the heaters were long enough

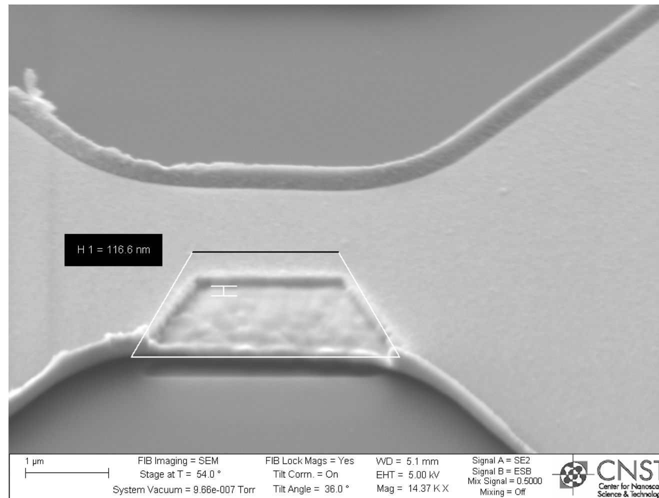

Figure 10.9 – SEM image of the first pass of the ion beam on the heater.

that it did not make much difference. Figure 10.10 shows some of the completed devices. The extra narrow trench is evident in the first picture where the fine beam was used to smooth the sidewalls. The device on the left was 268 nm and the one on the right was 232 nm.

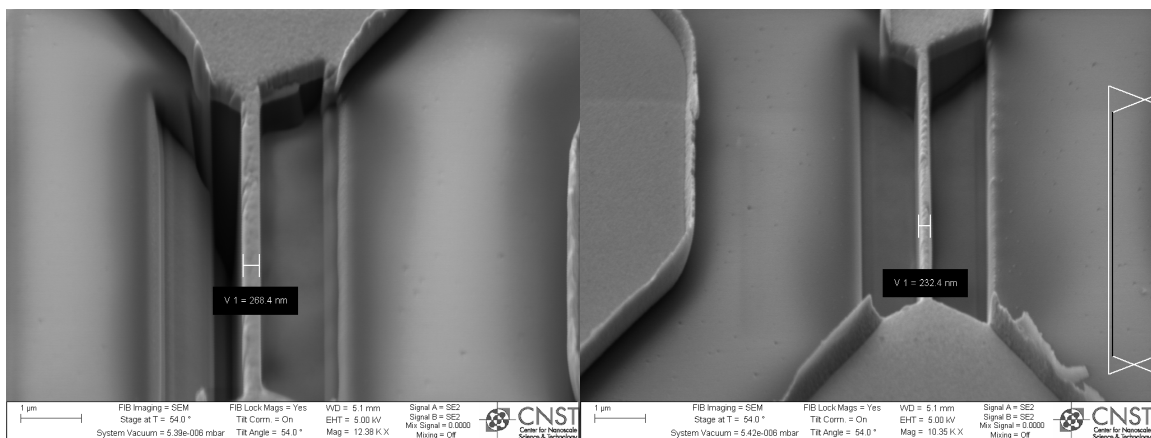

Figure 10.10 – SEM images of some of the finished devices.

Figure 10.11 shows the ground link severed by the FIB which removed the devices from the ground plane. Figure 10.12 shows a cross sectional view of the heater with the three layers on top of the silicon. One problem seen was that the thickness is now on the order of the width and appears rougher which means a bubble may form on the side and not on the top. Conversely, the thin silicon strip may be beneficial in that it will reduce the heat loss considerably.

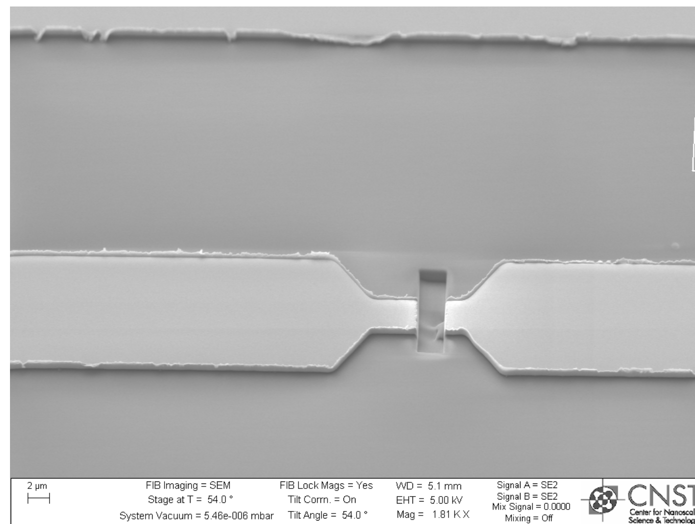

Figure 10.11 – SEM image of cut ground link.

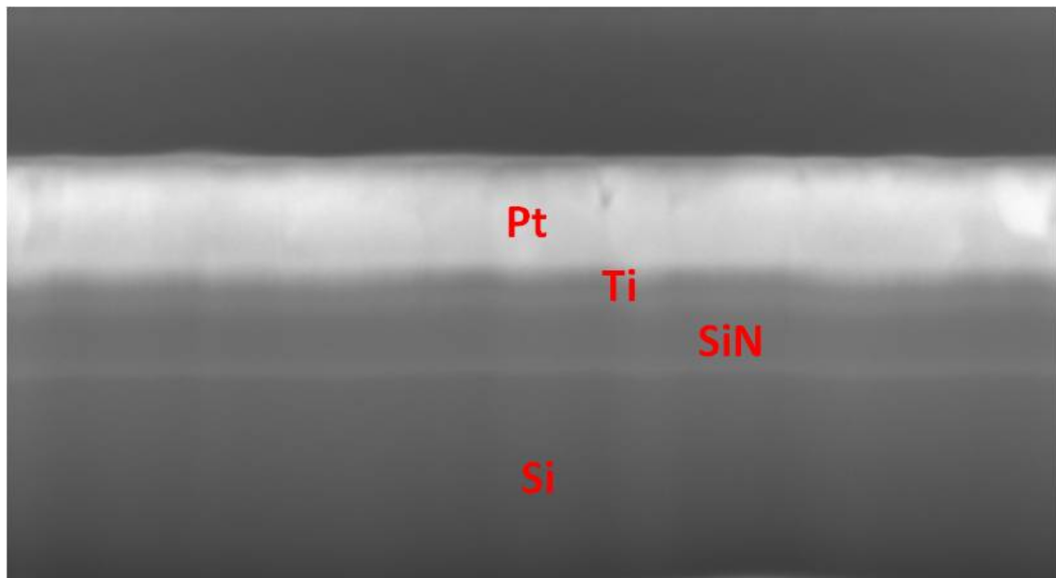

Figure 10.12 – Cross sectional view of the layers in the heater.

Testing

The reference 2 μm heater on the die worked fine and nucleated a bubble at around 8 volts. A 237 nm heater etched into an identical 2 μm heater failed when the voltage was stepped to 3.0 V without giving any evidence of boiling (inflection point). The data for this test is shown in Figure 10.13. The device failure was most likely the result of a single bubble forming on the side of the heater and then breaking

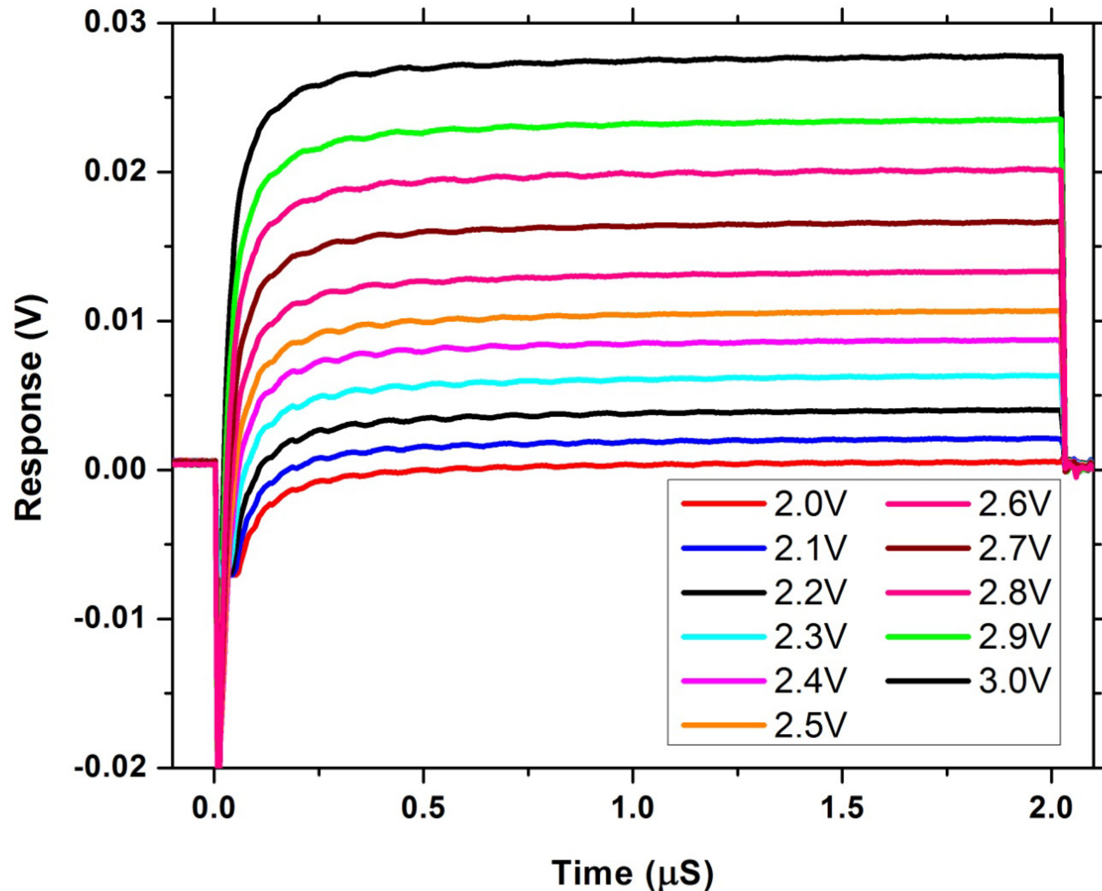

Figure 10.13 – Heater response vs. time for the 237 nm nanoheater.

the heater which has nothing behind it for support. From the heating curves it is not obvious if there is actually heating occurring. One way to tell is to plot the response vs. the input voltage. If the slope is linear then there is no heating occurring because the

resistance has not increased. Figure 10.14 shows that the slope is not linear which indicates that there is heating occurring at around 2.7 volts so more than likely there was a single bubble nucleated. This test was repeated for all of the devices and unfortunately the results were the same.

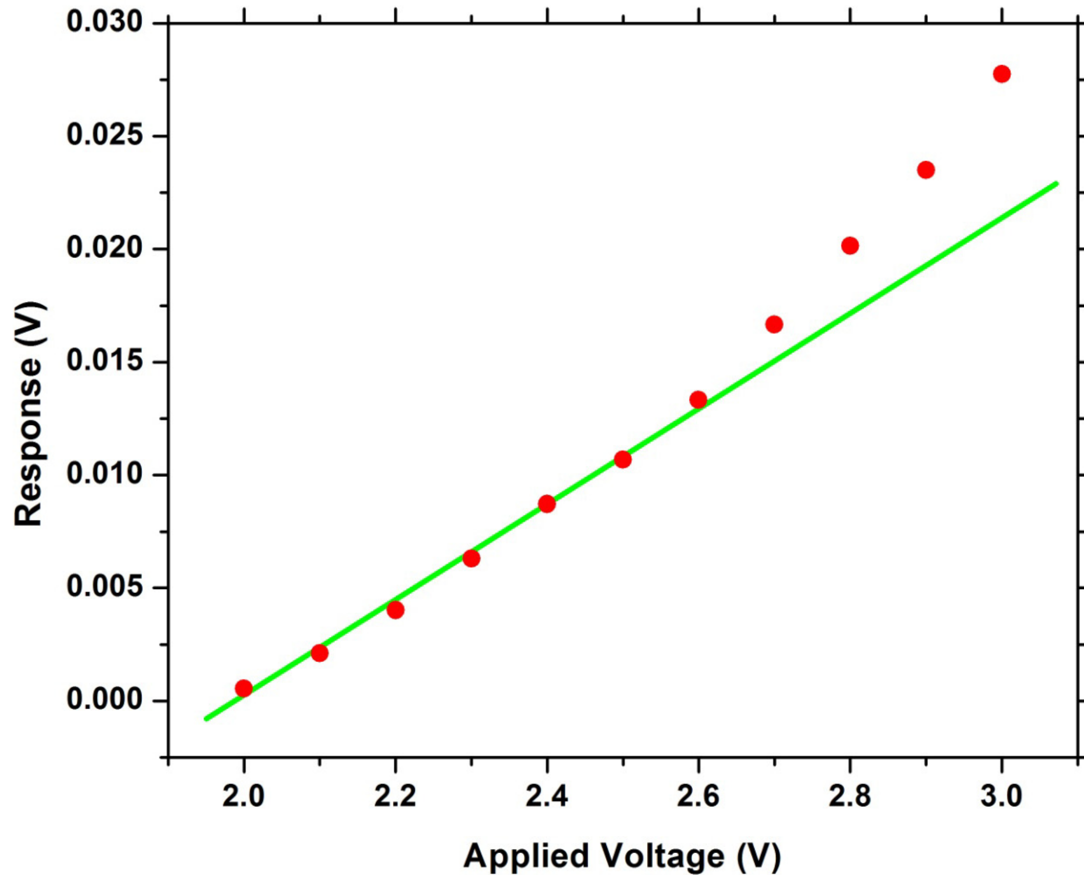

Figure 10.14 – Heater response vs. applied voltage at 1.9 μS showing an increase in resistance.

Chapter 11: Conclusions and Future Work

Conclusions

A series of microheaters of different widths and aspect ratios were fabricated. Systematic data showed that with decreasing width, the inflection point became more difficult to see on non-suspended devices. Backside etched devices were fabricated and were robust in repeated bubble nucleation events. The sensitivity of the nucleation measurements was dramatically increased and the power consumption was reduced by a factor of two over identical non-suspended heaters. While the nanoheaters did fail in initial tests when heated to the bubble nucleation temperature, the charging issues and fabrication issues were resolved.

New Applications

The processes developed in this work are being put to use on other novel devices. In a process called "Self Lithographic CVD Deposition", microhotplates are used in a CVD chamber to grow films on an array of heaters where each can be set to a different temperature. This can be done with these devices as well but with the added feature that the SiN membrane makes the device a Transmission Electron Microscope (TEM) grid so the films can be analyzed by simply placing the entire device in the TEM. We also expect to use this process to fabricate calorimeters on-a-chip

Future Work

Now that the sensitivity is increased there are many more liquids which our research group can investigate with these devices. For the first time, it will be possible, using the microboiling method, to measure the homogeneous nucleation temperature of many organic solvents. Looking at the data, there is one change that should be made to

reduce the power consumption of the devices. The current devices have connections to the bond pads that are 50 μm wide. This makes the resistance of the lines a much larger percentage of the resistance than the heaters which increases the power consumption. This was not a large problem in this work as the pulse generator could output very large voltages but it would be better to be able to use lower voltages. This may also fix some of the noise which was increasing as the heater widths increased. Figure 11.1 shows a new design that will be made later this year and uses 300 μm lines to make the lines approximately the resistance of the heaters as well as the length of each heater line the same.

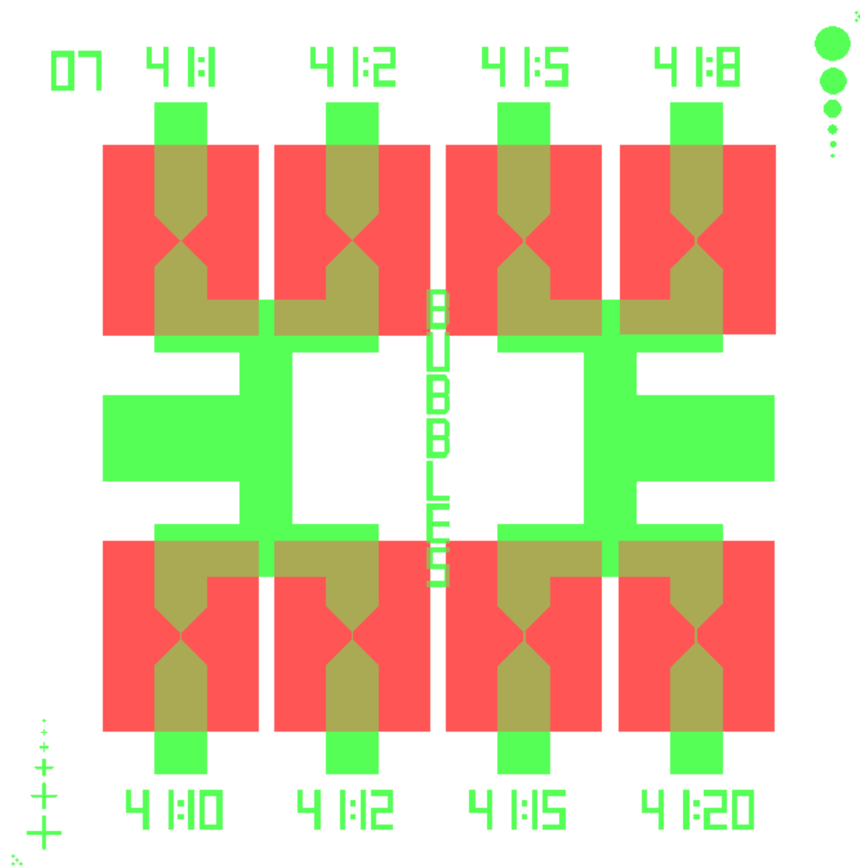

Figure 11.1 – New low resistance heater design.

Another new use of these devices is as a platform for the dropcasting of films. When a very small drop of material containing a particular film precursor is deposited on the device, the membrane forms a cup to hold the droplet in the center of the device as it is heated. When the liquid is evaporated, a thin film is left on the heater. Figure 11.2 shows some preliminary results of a film grown on one of the heaters from this wafer. On the left is a droplet of 25 mM $Sn(OH)_4$ sol-gel solution containing 30% glycerol. On the right is a SnO_2 film after annealing in air to 600 °C.

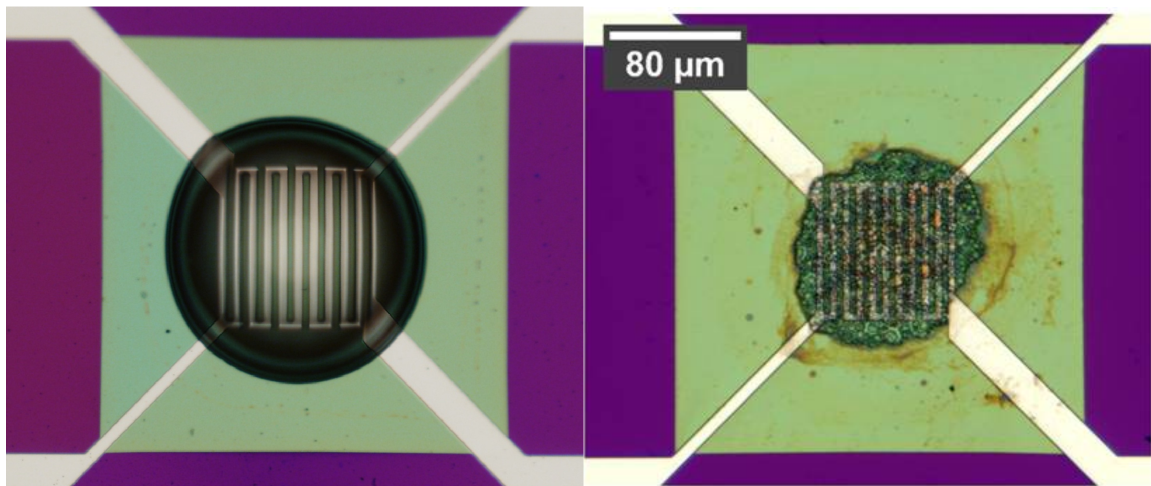

Figure 11.2 – SnO_2 film grown on suspended heater [24].

REFERENCES

[1] Cavicchi R.E. Private Communications (2008).

[2] Thomas, O. C.; Cavicchi, R. E.; Tarlov, M. J., Effect of surface Wettability on fast transient microboiling behavior. *Langmuir* **2003,** *19* (15), 6168-6177.

[3] Das, M.; Chatterjee, B. K.; Roy, B.; Roy, S. C., How high can the temperature of a liquid be raised without boiling? *Physical Review E* **2000,** *62* (4), 5843.

[4] Balss, K. M.; Thomas, O. C.; Avedisian, C. T.; Cavicchi, R. E.; Tarlov, M. J., Factors influencing microboiling behavior on gold microheaters. *Abstracts of Papers of the American Chemical Society* **2003,** *226*, 161-COLL.

[5] Balss, K. M.; Avedisian, C. T.; Cavicchi, R. E.; Tarlov, M. J., Nanosecond imaging of microboiling behavior on pulsed-heated Au films modified with hydrophilic and hydrophobic self-assembled monolayers. *Langmuir* **2005,** *21* (23), 10459-10467.

[6] Cavicchi, R. E.; Avedisian, C. T., Bubble nucleation and growth anomaly for a hydrophilic microheater attributed to metastable nanobubbles. *Physical Review Letters* **2007,** *98* (12), 124501/1-4.

[7] Avedisian, C. T.; Cavicchi, R. E.; Tarlov, M. J., Nanosecond Imaging of bubble nucleation on a microheater. *Journal of Heat Transfer-Transactions of the ASME* **2006,** *128* (8), 734-734.

[8] Avedisian, C. T.; Osborne, W. S.; McLeod, F. D.; Curley, C. M., Measuring bubble nucleation temperature on the surface of a rapidly heated thermal ink-jet heater immersed in a pool of water. *Proc. R. Soc. London Ser. A-Math. Phys. Eng. Sci.* **1999,** *455* (1991), 3875-3899.

[9] Avedisian, C. T.; Presser, C.; Stiehl, J.; Cavicchi, R. E., A simple method to assess the quenching effectiveness of fire suppressants. *Fire Saf. J.* **2010,** *45* (3), 206-210.

[10] Deng, P.; Lee, Y.-K.; Cheng, P., An experimental study of heater size effect on micro bubble generation. *International Journal of Heat and Mass Transfer* **2006,** *49* (15-16), 2535-2544.

[11] Suehle, J. S.; Cavicchi, R. E.; Gaitan, M.; Semancik, S., Tin Oxide Gas Sensor Fabricated Using CMOS Micro-Hotplates and Insitu Processing. *IEEE Electron Device Lett.* **1993,** *14* (3), 118-120.

[12] Robert Bosch Gmbh, U.S. Patent 4,855,017 and 4,784,420

[13] Zhenjun, Z.; Chang, L. In *An efficient PC-based preferential-etch simulator using dynamic cellular automata method*, Solid-State and Integrated Circuit Technology, 1998. Proceedings. 1998 5th International Conference on, 1998; 1998; pp 943-946.

[14] Wafer Holder Brochure — Single With Backside Protection - Advanced Micromachining Tools
http://www.ammt.com/content/__papers/AMMT_PI_WESingle.pdf

[15] Seidel, H.; Csepregi, L.; Heuberger, A.; Baumgartel, H., Anisotropic etching of crystalline silicon in alkaline solutions, 1. Orientation dependence and behavior of passivation layers. *J. Electrochem. Soc.* **1990,** *137* (11), 3612-3626.

[16] Shipley Microposit LOL 1000 Datasheet

[17] Golden, J.; Miller, H.; Nawrocki, D; Ross, J. Optimization of Bi-layer Lift-off Resist Process. *CS Mantech Technical Digest*, http://www.csmantech.org/Digests/2009

[18] Montgomery, C.B. Private Communications (2011).

[19] "Electrical Resistivity of Pure Metals," in CRC Handbook of Chemistry and Physics, 91st Edition (Internet Version 2011), W. M. Haynes, ed., CRC Press/Taylor and Francis, Boca Raton, FL.

[20] Henein, G.E. Private Communications (2010).

[21] Novotny, D.B. Private Communications (2009).

[22] Machunze, R.; Janssen, G., Stress gradients in titanium nitride thin films. *Surf. Coat. Technol.* **2008,** *203* (5-7), 550-553.

[23] Firebaugh, S. L.; Jensen, K. F.; Schmidt, M. A., Investigation of high-temperature degradation of platinum thin films with an in situ resistance measurement apparatus. *J. Microelectromech. Syst.* **1998,** *7* (1), 128-135.

[24] Rogers, P.H. Private Communications (2011).